INSTITUTO SUPERIOR DE ENGENHARIA DO PORTO
MESTRADO EM ENGENHARIA MECÂNICA




NUMERICAL THERMOMECHANICAL ANALYSIS OF SCARF ADHESIVE JOINTS

JORGE AUGUSTO DIAS SOUSA
outubro de 2023

POLITÉCNICO
DO PORTO

Instituto Superior de Engenharia do Porto

NUMERICAL THERMOMECHANICAL ANALYSIS OF SCARF ADHESIVE JOINTS

Jorge Augusto Dias Sousa

2023

ISEP – School of Engineering

Department of Mechanical Engineering

P.PORTO

Instituto Superior de Engenharia do Porto

NUMERICAL THERMOMECHANICAL ANALYSIS OF SCARF ADHESIVE JOINTS

Jorge Augusto Dias Sousa

1160511

Dissertation presented to School of Engineering to fulfil the requirements necessary to obtain a Master's degree in Mechanical Engineering, carried out under the guidance of Raul Duarte Salgueiral Gomes Campilho, PhD.

2023

ISEP – School of Engineering

Department of Mechanical Engineering

P.PORTO

ACKNOWLEDGEMENTS

Foremost, I would like to express my immense gratitude to my advisor Professor Raul Campilho, PhD, for all the support in my research, for his patience, motivation and knowledge, for all the hours he was present guiding me, for all the help throughout this project.

I cannot forget to mention my parents, who were the ones who made it all possible. Without them I wouldn't even be here.

And last but not least, I want to thank my girlfriend, hopefully future wife, for all the patience and unslept hours hearing and helping me the best way she could.

ABSTRACT

Given the industrial demands presented nowadays, adhesive bonding is a concept that goes towards the needs of the future. It is a process that is evolving too fast in order to keep up with it. It is replacing other traditional methods, not only because of its improved stress distribution and improved stiffness, but also because it can be used in high strength and lightweight structures at lower cost and easier production, among other advantages. Adhesive joints can come in different formats such as lap joints, butt joints or strap joints, just to name a few. The scarf adhesive joint belongs to the butt joints type configuration and it allows smoother surfaces, and some research has been done to this type of joint.

Most structures must endure challenging conditions and temperature can be a disruptor of performance. Thus, this dissertation aims to study the effect of temperature in adhesive joints and understand the material and geometric factors that can influence it. The focus will be on scarf adhesive joints in a numerical thermo-mechanical analysis. Temperature has a significant effect on the adhesive and on the interface of the adhesive joint. The thermal effects will be studied in scarf joints with various scarf angles, from 3.43° to 45°, with three different adhesives, the Araldite® AV138 (brittle epoxy), the Araldite® 2015 (reasonable ductile epoxy) and the Sikaforce® 7752 (ductile polyurethane). With the support of the Abaqus software and cohesive zone modelling, a two-step thermo-mechanical analysis will be used to determine the temperature effects and understand the respective joint behaviour.

The main conclusions of the present work are as follows:

- The lower the scarf angle, the higher the bonded area; therefore, the joint strength increases;
- The higher the temperature, the higher the joint displacement to failure;
- Temperature also influenced stress levels (both shear and peel), and this effect is more noticeable as scarf angles are increased;
- Temperature does not affect maximum force;
- Cohesive Zone Modelling is a precise technique in predicting strength of various joint configurations and adhesives.

KEYWORDS

Adhesive bonding, scarf adhesive joint, temperature, numerical thermo-mechanical analysis, scarf angle.

RESUMO

Dadas as exigências industriais atuais, a ligação adesiva é um conceito que vai ao encontro das necessidades do futuro. É um processo que está a evoluir a um ritmo significativo e tem vindo a substituir outros métodos tradicionais, não só devido à sua melhor distribuição de tensões e maior rigidez, mas também porque pode ser utilizada em estruturas de elevada resistência e leveza, com custos mais baixos e produção mais fácil, entre outras vantagens. As juntas adesivas podem apresentar-se em diferentes formatos, tais como juntas sobrepostas, juntas de topo ou juntas de cinta, só para citar alguns. A junta adesiva tipo cachecol pertence à configuração das juntas de topo e permite superfícies mais suaves, tendo sido efetuada alguma investigação sobre este tipo de junta.

A maioria das estruturas tem de suportar condições difíceis e a temperatura pode ser um fator de perturbação do desempenho. Assim, esta tese tem como objetivo estudar o efeito da temperatura em juntas adesivas, e compreender os materiais e os fatores geométricos que a podem influenciar. O foco será nas juntas adesivas de chanfro interior numa análise numérica termomecânica. A temperatura tem um efeito significativo no adesivo e na interface da junta adesiva. Os efeitos térmicos serão estudados em juntas de chanfro interior com vários ângulos, desde 3.43° até 45°, com três adesivos diferentes, o Araldite® AV138 (epóxi frágil), o Araldite® 2015 (epóxi dúctil razoável) e o Sikaforce® 7752 (poliuretano dúctil). Com o apoio do software ABAQUS e da modelação da zona coesiva, será utilizada uma análise termomecânica em duas fases para determinar os efeitos da temperatura e compreender o respetivo comportamento da junta.

As principais conclusões do presente trabalho são as seguintes:

- quanto menor for o ângulo do chanfro interior, maior será a área de ligação adesiva; por conseguinte, a resistência da junta aumenta;
- quanto maior for a temperatura, maior será o deslocamento da junta até à rotura;
- a temperatura também influenciou os níveis de tensão (tanto de corte como de arrancamento), e este efeito é mais notório à medida que os ângulos de chanfro interior aumentam;
- a temperatura não afeta a carga máxima;
- o Modelo de Danos Coesivo é uma técnica precisa na previsão da resistência em juntas de várias configurações e adesivos.

PALAVRAS-CHAVE

Ligação adesiva, junta adesiva de chanfro interior, temperatura, análise numérica termomecânica, ângulo do chanfro interior.

INDEX

FIGURES INDEX

TABLES INDEX

LIST OF ABBREVIATIONS AND SYMBOLS

List of abbreviations

BJ	Butt Joint
BLJ	Bevelled Lap Joint
CS	Coefficient of Swelling
CTE	Coefficient of Thermal Expansion
CZM	Cohesive Zone Modelling
DLJ	Double Lap Joint
DSC	Differential Scanning Calorimetry
FEM	Finite Element Method
FTIR	Fourier Transform Infrared
HT	High Temperature
LT	Low Temperature
PU	Polyurethane
RIM	Reaction Injection Moulded
RT	Room Temperature
SDEG	Stiffness Degradation
SJ	Scarf Joint
SLJ	Single Lap Joint
TGA	Thermogravimetric Analysis
UTS	Ultimate Tensile Strength

List of symbols

ΔT	Temperature differential	°C
Al	Aluminium	
E_{diss}	Dissipated energy	kN.mm
σ	Force per area	MPa
P	Force	N
P-δ	Force-displacement	
P_{max}	Maximum force	N
T	Temperature	°C
T_g	Glass-transition temperature	°C

1. INTRODUTION

1.1. Framework

Adhesive bonding is a more established concept of joining materials. It is a very sought process that is developing at a rapid pace to keep up with the industrial demands.

Therefore, adhesive structures must be able to withstand severe conditions as temperature. This is a factor that can have a significant influence in all types of materials and constructions.

Moreover, it is important to be aware of the challenges that temperature can bring. In uncontrolled environments, it can change anytime, anywhere. The variability of temperature can be a factor of destabilisation as well as low or high temperature exposure can also be.

1.2. Goals

The aim of this work is to understand the effect of temperature in adhesive joints and prepare the next phase, in which a numerical study will be conducted in scarf adhesive joints using the FEM software ABAQUS®. Several simulations of thermal environments will be carried out.

1.3. Dissertation's structure

This work is divided in four main chapters:

- In the first chapter starts there is a contextualisation of the work and the goals are outlined;
- In chapter 2, the basis of the work is described from the introduction in scarf adhesive joints to the effects of temperature in joints. Strength prediction techniques are also discussed;
- In chapter 3, the work is presented from the procedures of the simulations to a presentation of the results, through various forms of analysis;
- Chapter four englobes a critical analysis of chapter 3, in which all the main concepts and conclusions are presented.

All the necessary references and sources for the bibliographic work are listed in chapter 5.

2. STATE OF THE ART

2.1. Adhesively-bonded scarf joints

2.1.1. Design and applications

The scarf joint (Figure 1) is the most elegant joint [1], it is an overlap joint in which the angle (α) between the axis of the adhesive layer and the axis of the adherends (of equal width and thickness) is greater than 0° (butt joint) and less than 90° [2]. Therefore, the thickness remains constant at the joint section [3] [4]. This joint design is frequently applied in the construction of huge composite structures or in the repairing of damaged sections [3] [4].

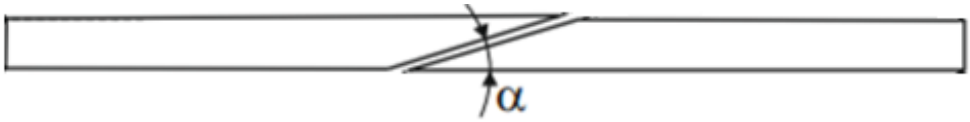

Figure 1 - Geometry of a scarf adhesive joint.

2.1.2. State-of-the-art

EFFECT OF ADHESIVE THICKNESS, ADHESIVE TYPE AND SCARF ANGLE ON THE MECHANICAL PROPERTIES OF SCARF ADHESIVE JOINTS [5]

Liao et al. studied adhesive thickness, adhesive type and scarf angle in the performance of scarf adhesive joints through the application of uniaxial tensile load. The material parameters of the adherends are like a high-strength steel.

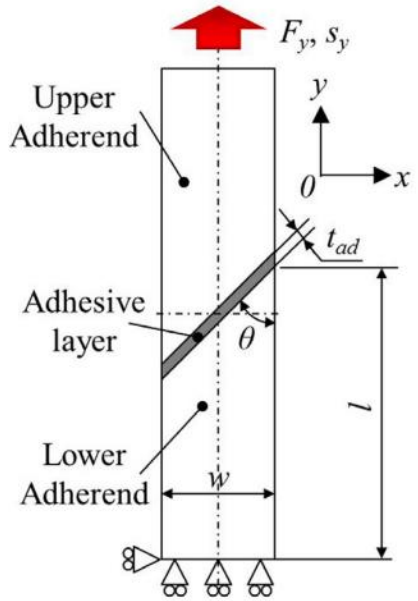

Figure 2 - Geometries and variables of the model SJ [5].

The main conclusions are:

- the ultimate tensile loading increases as adhesive thickness decreases;

- load-bearing capacity of the joint is affected by adhesive type as is lost with a brittle adhesive and partially sustained with a ductile adhesive;
- maximum applied displacement is proportional to the adhesive thickness with a ductile adhesive;
- failure energy increases as adhesive thickness decreases with a brittle adhesive. It is vice-versa for the ductile adhesive;
- as scarf angle decreases:
    - adhesive thickness effect is more pronounced;
    - the ultimate tensile loading, the maximum applied displacement, and the failure energy increase.

EXPERIMENTAL AND NUMERICAL ANALYSIS OF SCARF ALUMINUM ADHESIVE JOINTS [6]

Silva et al. worked on the validation of CZM laws in traction and shear. The model in aluminium AW6082-T651 bonded with three different adhesives (AV138, Ar2015 and SK7752) and various scarf angles. Like in the previous study [5], adhesive type and scarf angle belong to the main control parameters of the mechanical properties of a SJ.

EFFECTS OF BONDLINE FLAWS ON THE DAMAGE TOLERANCE OF COMPOSITE SCARF JOINTS [7]

Goh et al. studied the effect of different length disbonds on the strength of secondarily bonded composite SJs. Experimental testing, analytical modelling and numerical simulation were conducted. The conclusions are that:

- the size of the bondline flaw is more influential in the reduction of the load-carrying capacity than the decrease in the effective bond area;
- the ply angle adjacent to the crack and the size of the flaw are the main factors in the complete fracture strength;
- the fracture occurred in the composite adherend at an equal distance to a small fraction of ply thickness and it was primarily by:
    - matrix shear failure in the 0° and 45° and
    - matrix peel failure in the 90°;
- CZM is accurate for all the flaw sizes considered.

OPTIMISATION STUDY OF TAPERED SCARF AND STEPPED-LAP JOINTS IN COMPOSITE REPAIR PATCHES [8]

Bendemra et al. did a parametric study using a linear finite element analysis to investigate the influence that joint design parameters (such as ply thickness, adhesive thickness, taper angle, stacking sequence, overply layup, and overply lap length) have on peak stresses in the adhesive bondline of tapered scarf (Figure 3) and stepped-lap joints.

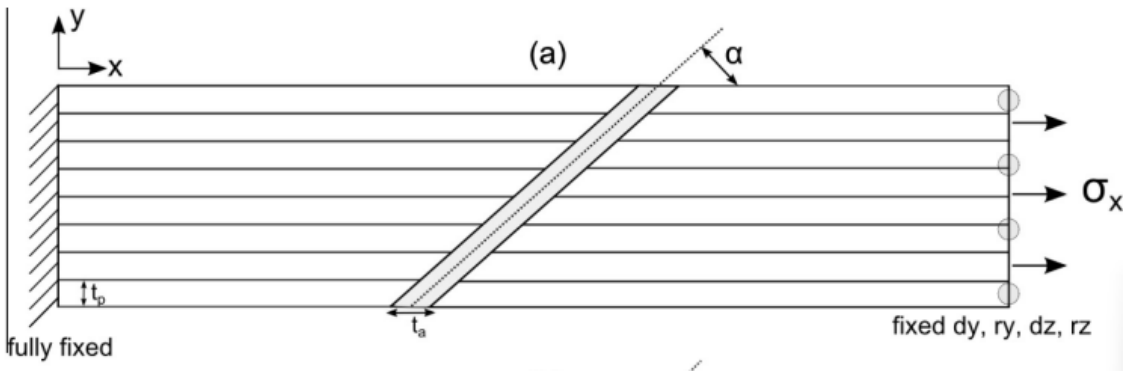

Figure 3 - Geometry of SJ specimen in study [8].

The main conclusions are that:

- peak peel and shear stress on the joint configurations in study are prone to ply thickness, taper angle and stacking sequence;
- the overplies that were introduced gave protection and stiffness at joint tips and, therefore, an overply lap length so peak stresses won't increase;
- and also, it can offset the high stress concentration in stepped-lap joints which are higher in this joint configuration than the equivalent tapered SJs;
- the location of 0° plies in the composite laminates is an important factor due to high stress concentration in the adhesive region adjacent to 0° plies.

2.2. Joints submitted to temperature

2.2.1. Background

The effect of temperature in adhesive joints is in study, therefore, there's an introduction to temperature in adhesive bonding, a description of the principles that will be used on the numerical modelling and two-part state-of-the-art (experimental and numerical.

2.2.2. Features

Adhesive bonding is an established method of joining materials which most industries are using. Nonetheless, the demands are always increasing. Temperature can also be a stress factor and thermal stresses are significant in thermal expansion gradients. It is important to have the ability to withstand large gradients of temperature. The polymeric nature of most of the structural adhesives does not perform as well as mechanical methods in conditions of extreme temperature gradients. When joints are submitted to temperature, there are conditions that must be considered:

- adhesive shrinkage,
- CTEs,
- creep and
- joint design.

Adhesive (layer) shrinkage is a cure byproduct. It depends on the method of cure, on the chemical structure of the adhesive and on the forces of attraction that occur in the cure process. Hot-cure adhesives have low shrinkage while water absorption ones have no shrinkage. Stresses are insignificantly small; however, post-cure distortion can happen and it should be managed.

Most materials can contract and expand. This phenomenon is defined by the CTE. In a single material, the consequent stress is not a factor. However, in general, adhesives have higher CTEs than adherends, therefore they can contract more. Cooling after an elevated temperature curing cycle is often the most incisive temperature change. Thermal stresses can also occur in adherends with different CTEs. The substrate with higher coefficient will compress the other. The transmission of internal load induces shear stress through the adhesive. It can cause joint failure without applying any load. If the adherends have the same CTE, the adhesive does not transmit internal load. The adherends block thermal contraction (of the adhesive). A longitudinal tensile direct stress is formed in the adhesive due to the shear stress along the interface (at the overlap). These stresses are much lower than those of substrates with different CTEs.

Viscoelasticity is a property of some materials, e.g., polymer-based adhesives. These materials have time-dependent stress-strain behaviour for static loads [16] and creep is a time-dependent total stress deformation, which is not applicable for instant deformation. Thermal loading is prone to cause creep failure, but it is difficult to predict it [16]. Therefore, the combination of CTE mismatches and viscoelasticity can cause thermal stress concentration [16].

Curing and service temperature of most adhesives are higher than Tg; thus, thermal stresses are rare. In joints of metal or composite substrates bonded with a stiff adhesive, thermal stresses are high. It is not recommended to use soft adhesives in large bonding areas and thin bondlines.

The stress analysis for mechanical loading can be readily modified to incorporate thermal stresses.

2.2.3. Principles of numerical modelling

In most cases, studies made in adhesive joints about thermal stresses and strain distribution have presumptions, such as,

- the convective heat transfer is ignored;
- the temperature distribution is uniform;
- or the transient temperature distribution is not considered.

In the numerical modelling of joints submitted to temperature,

- the outer surfaces of the adhesive joint are subject to fluid flows in different temperature and velocity [9];
- it must be applied initial uniform joint temperature and convective heat transfer as boundary conditions [10],
- the adherends have different edge conditions [9];
- a steady state heat transfer [10],

These allow to obtain the final temperature distribution in the adhesive joint [10]. However, it should be known that there are two aspects to consider about heat transfer.

- the convection from fluid to adherends or adhesive (from the joint surfaces to the fluids, or the fluids to the joint surfaces); [10] [9]
- and the conduction through adherends and adhesive (throughout the adhesive joint) [10] [9].

The convective heat transfer is dependent on the heat transfer coefficient [9]. Also, the convective heat transfer coefficients are computed for each surface because of dissimilar geometries and air flow [10].

In the meshing, there are no defects, e.g., air hole, residual stresses in the SLJ and the interface bond strength is competent (through appropriate selection of the adhesive) [10]. The level of refinement influences the accuracy of local stresses or strains. These are more critical near the adhesive fillets and the adhesive layer, therefore, a local mesh refinement [10].

Thermal strain distributions in the adhesive SLJ are dependent on the temperature distributions, therefore, the joint must be first heated (thermal analysis) and then, the geometrically non-linear stress analysis of the adhesive joint (based on the small strain–large displacement theory) [9].

2.2.4. State-of-the-art

A spotlight on the experimental and numerical work done, respectively, to study the effects of temperature on adhesive joints in different configurations with different materials is presented in two parts.

2.2.4.1. Experimental work

EFFECT OF TEMPERATURE ON THE MECHANICAL PROPERTIES OF ADHESIVELY BONDED BASALT FRP-AL ALLOY JOINTS IN THE AUTOMOTIVE INDUSTRY [11]

Na et Al. studied the effect of temperature on the mechanical properties of adhesively bonded BFRP-Al joints. Several joint configurations (Figure 4) were shear loaded such as bulk tensile specimens, BJs, 45° SJs and thick adherend shear joints (TASJs). The adhesive for the study was a two-part Araldite® 2015, an epoxy adhesive. The applied temperatures were -40, -10, 25 (RT), 50 and 80°C.

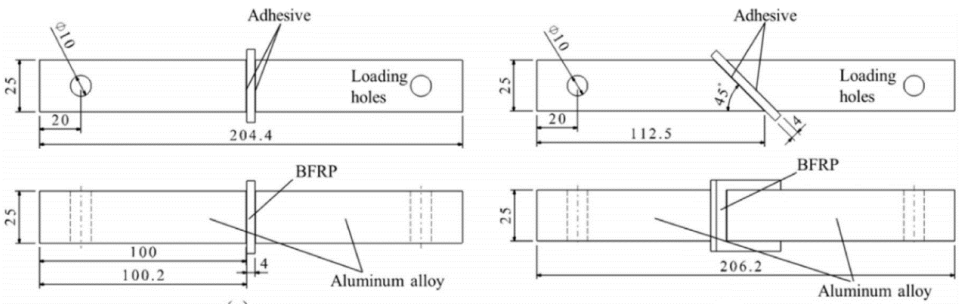

Figure 4 - Geometries and dimensions (in mm) of adhesive joints. BJ, on the left and SJ, on the right [11].

It was concluded that the mechanical properties of the adhesive were affected by temperature. As temperature increased, the adhesive became more ductile and properties like Young's modulus

and tensile strength decreased while tensile strain increased. These effects were more pronounced at temperatures close to *Tg*. In contrast, at low temperatures, the adhesive was in glass state and temperature was almost a no factor.

For the strength of the joints, it was concluded that either the adhesive or the composite properties are the factors. The joint's shear load capacity reaches its highest. The three (studied) joint configurations had decreasing failure strength with increasing temperature, sharper at HTs. As temperature decreased, delamination and fibre breakage could occur in BFRP. In normal stress state, it was observed that complete delamination failure often happened. It was advised to avoid the normal and complex stress state. Therefore, temperature and stress state were the modes for failure.

In the end, it was proposed to study the mechanical properties of:

- BFRP at different temperatures
- and joints with dissimilar CTEs adherends.

ADHESIVE JOINTS USING ALUMINIUM AND CFRP SUBSTRATES TESTED AT LOW AND HIGH TEMPERATURES UNDER QUASI-STATIC AND IMPACT CONDITIONS FOR THE AUTOMOTIVE INDUSTRY [12]

Machado et Al. studied the behaviour of dissimilar (CFRP and Al - 5754-H22 and 6060-T6) SLJs with the intent to understand and predict it. Several joint (Figure 5) combinations were tested at temperatures that ranged from −30°C to 80°C under quasi-static and impact loads (all compliant with automotive industry requirements).

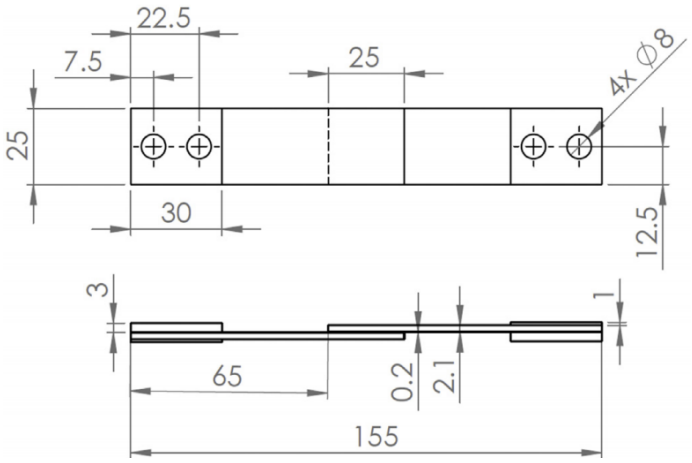

Figure 5 - Geometry and dimensions (in mm) of SLJs specimens [12].

For similar adhesive joints, it was concluded that CFRP-CFRP had the highest failure load at almost all conditions. In impact conditions, the frictional sliding that occurred in delamination increased the energy absorption to the most of all. However, as temperature decreased, Al joints absorb more energy. Al joints had considerably lower failure loads and displayed low sensitivity to temperature. In quasi-static conditions, the energy absorption was the highest at all temperatures. In impact conditions, the failure occurred at the grip, representing a cohesive failure of the adherend, which is the most ideal.

For the dissimilar joints, Al deformation was the limiting factor at maximum load for all conditions.

WET THERMO-MECHANICAL BEHAVIOUR OF STEEL-CFRP JOINTS - AN EXPERIMENTAL STUDY [13]

Agarwal et Al. studied the effect of steel-CFRP SLJs exposed to wet thermal cycle ranges and sustained (shear) loads. The thermal cycling ranges were 10°C to 40°C and 10°C to 50°C and the sustained loads were 30% and 50% of the short-term bond strength. The goal was to investigate the effects of different environmental and loading scenarios on the long-term strength and durability of the test specimens.

The specimens (Figure 6) were tested under different loading scenarios such a) control specimens under instantaneous load and ambient conditions, b) sustained load only under ambient conditions, c) wet thermal cycling only (no mechanical load) and d) both sustained load in immersed conditions.

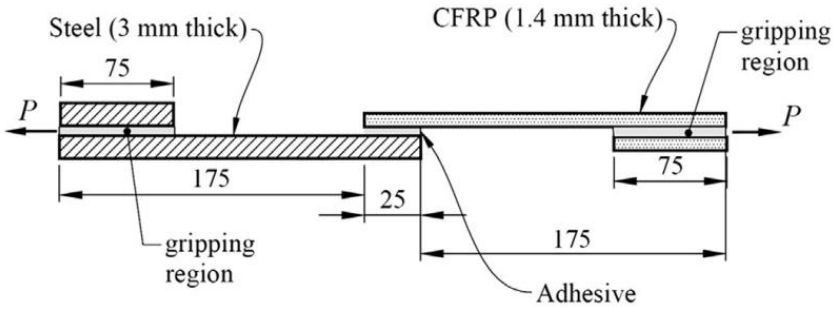

Figure 6 - Dimension of steel-CFRP single lap shear specimen (in mm) [13] [14].

It was concluded that the bond strength of the test specimens is not reduced significantly for condition *b*, 50% for 21 days. In condition *c*, 108 cycles between 10°C and 50°C reduced peak bond strength in 15% and failure mode was interfacial debonding. In the other cycle, the failure mode changed to delamination. For condition *d*, all test specimens sustained up to 15 thermal cycles and failed because of steel-adhesive interfacial degradation. In this condition, only at 30% of sustained load between 10°C and 40°C is that the 108 cycles are sustained. The bond strength is reduced up to 47% and failure was delamination. In the end, the influence of condition *d* was critical.

TESTING OF NEW ADHESIVE AND CFRP LAMINATE FOR STEEL-CFRP JOINTS UNDER SUSTAINED LOADING AND TEMPERATURE CYCLES [14]

Agarwal et al. tested a new adhesive and CFRP laminates for steel-CFRP joints. The joints were tested under sustained (shear) loading and temperature cycle. The goal was to investigate the effects of different environmental [13] and loading scenarios on the long-term strength and durability of the test specimens [13]. The dimension of the specimens is the same as in Figure 6.

The test conditions were the same as [13] plus a test of both sustained load and thermal cycle in dry conditions. The applied sustained loads were also de same [13]. However, in this study, only one thermal cycle was applied, and it ranged between 10°C and 50°C.

In test condition *c* [13] for 21 days, the residual strength decreased around 16% which was like the results of their previous work. In condition *d* [13] for sustained load of 50%, there was not residual bond strength degradation unlike previous work. The *Tg* of the adhesive is 32°C higher than the maximum temperature. In literature, this value is recommended to be 20°C to 30°C higher than the service temperature.

It was observed that the failure mode in all specimens under wet thermal cycling conditions *c* and *d* was interfacial debonding failure. The steel-adhesive interface was identified as the critical link for failure. There was a necessity for testing condition *e*, the test specimens were waterproof coated and sealed. The effect of moisture was tested, and the results were similar to those obtained in conditions *c* and *d*. However, there was delamination failure as occurred in conditions *a* and *d*. It was concluded that the interface was degraded by moisture instead of thermal cycling. In the end, it was advised to waterproof the joints in wet conditions.

EFFECT OF CONTINUOUS HIGH TEMPERATURE EXPOSURE ON THE ADHESIVE STRENGTH OF EPOXY ADHESIVE, CFRP AND ADHESIVELY BONDED CFRP-AL ALLOY JOINTS [15]

Qin et al. studied the effect that a 30-day continuous exposure to HTs (80°C with extremely low relative humidity) had on the strength of an epoxy adhesive (Araldite® 2015), CFRP and CFRP-Al bonded joints. The goal was to investigate the degradation mechanism of the joints. Several configurations were used, TSJs, 45° SJs (Figure 7) and BJs. The study consisted in exposing the test specimens to temperature, and after it, a tensile stress test was realised. In between, several analyses were made, FTIR, DSC and TGA.

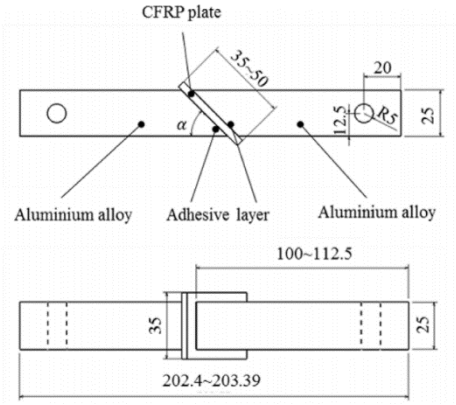

Figure 7 - Geometries and dimensions (in mm) of SJs [15].

It was concluded that the thermal behaviour of the adhesive was post curing. It was also detected that thermal exposure:

- degraded CFRP as shear and normal strength decreased almost 40%. The improvement of surface roughness can reduce this value to approximately 10%, e.g., sandpaper polishing;
- changed the epoxy matrix and decreased interlaminar strength as shown by large interface and delamination failure;
- increased the failure strength and Young's modulus of the bulk specimens by approximately 60% and decreased tensile failure strain;
- was more pronounced with increasing proportion of normal stress in the bondline. So, the extents of shear and normal strength were different.

In the end, the dissimilar joints deterioration was mainly due to CFRP degradation and interface failure.

2.2.4.2. Numerical modelling

ON NON-LINEAR THERMAL STRESSES IN AN ADHESIVELY BONDED SLJ [9]

Apalak and Gunes studied non-linear thermal stresses in SLJs (medium carbon steel, 1040, and rubber modified epoxy adhesive). It was assumed that the outer surfaces were subject to air flows with different temperatures and velocities, and large displacement effects were considered. The geometrical analysis was done with ANSYS software and used the incremental FEM in four adherend edge conditions (Figure 8). In this study, the premise was "the adhesive and adherends present different stress and strain states under thermal loads due to the thermomechanical mismatches".

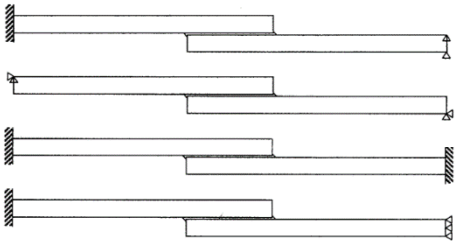

Figure 8 - Boundary conditions of the SLJ [9].

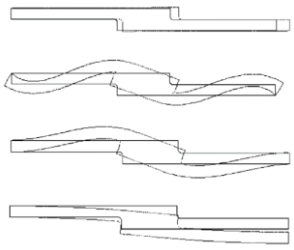

Figure 9 - Deformed geometries for the end conditions [9].

It was concluded that thermal loads, like structural loads, caused significant stress and strain concentration in the interfaces, peaking at the adhesive free ends. These stresses can exceed the yield point. The same occurred for the thermal and mechanical mismatches of the joint's members resulted in significant strain concentrations in the interfaces. And it was found that overlap length increase had not an impact in decreasing peak stresses.

In the end, it was advised that variable thermal conditions must be taken into consideration in the design process.

NUMERICAL ANALYSIS ON THE TEMPERATURE AND THERMAL STRESS DISTRIBUTION IN ADHESIVE JOINTS [10]

Zhao et al. used the finite element method to numerically analyse the temperature distribution of (medium carbon steel substrates and epoxy adhesive) SLJs (Figure 10). It was assumed that the outer surfaces were subject to air flows with different temperatures and velocities (Figure 11) [9]. The effects of end condition, thickness and overlap length were included in the analysis. The goal of this study was to use the results for strength prediction and design optimisation.

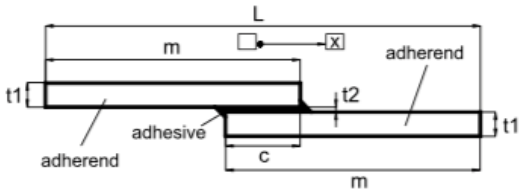

Figure 10 - Dimensions of the SLJ, t1=2mm, t2=0,2mm, m=30mm and c=5mm [10].

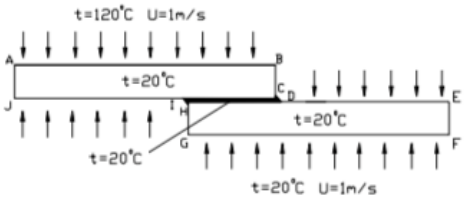

Figure 11 - Thermal boundary conditions of SLJ [10].

It was concluded that the increase of adhesive thickness increased temperature in the mid-bondline and improved thermal stress distribution which was beneficial. However, thermal stress in the adhesive was still higher at the free ends than at the centre and it could lead to cracking. The end conditions were influent on the thermal stress, e.g, large and moderate rotation could cause high and low stress, respectively. It also influenced the overlap length effect on thermal stresses, however, overlap length did not have a significant impact on the mid-bondline temperature [9].

2.3. Strength prediction techniques for adhesive joints

This section presents an overview of the most relevant analytical and numerical methods for the strength prediction of bonded joints. The analytical analysis of bonded joints began about eighty years ago with Volkersen [16]. This model is an analytical approximation based on a simple model of a SLJ. After being presented, this model has been continuously improved to approach the real behaviour of bonded joints [17].

2.3.1. Analytical methods

Volkersen's method [16] is the most simple and limited method to obtain shear stresses in a SLJ. This solution is represented in Figure 12. Shear stresses in the adhesive are maximum at the overlap edges and minimum at the inner portion of the bond.

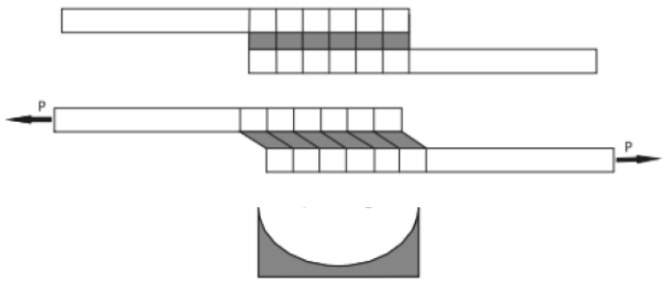

Figure 12 - Specimen without load (up), specimen with load (middle), shear stress in adhesive layer (down) [18]

The Goland and Reissner's [19] analysis took into account the fact that the load (*P*) in Figure 12 is non collinear, therefore creating a bending moment that promotes the joint's transverse deflection. The displacements are no longer proportional to the load, which results in a geometrical non-linearity. The results of this model were very similar to those of Volkersen regarding shear stresses, but this analytical formulation also allows to obtain peel stresses, as shown in Figure 13.

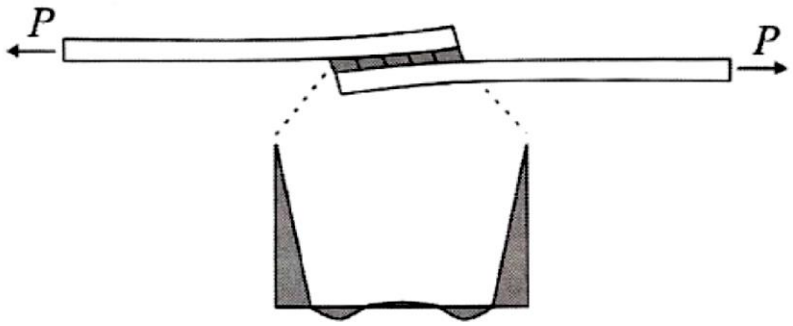

Figure 13 - Peel stresses in the adhesive by the Goland and Reissner's analysis [18]

The analysis of Hart-Smith [20] goes further and considers that, beyond elastic deformation, adhesives and adherends also have plastic deformations. This method shows that the adhesive's plasticity increases the strength of a joint compared with an elastic analysis because, when the material plasticizes, a redistribution and a peak reduction of stresses occur, and failure takes longer to occur. Hart-Smith chose an elasto-plastic model and showed that the actual form of the adhesive´s *P-δ* curve was less important than the area under it (which represents the dissipated energy). Therefore, an elastic-perfectly plastic response was assumed (Figure 14).

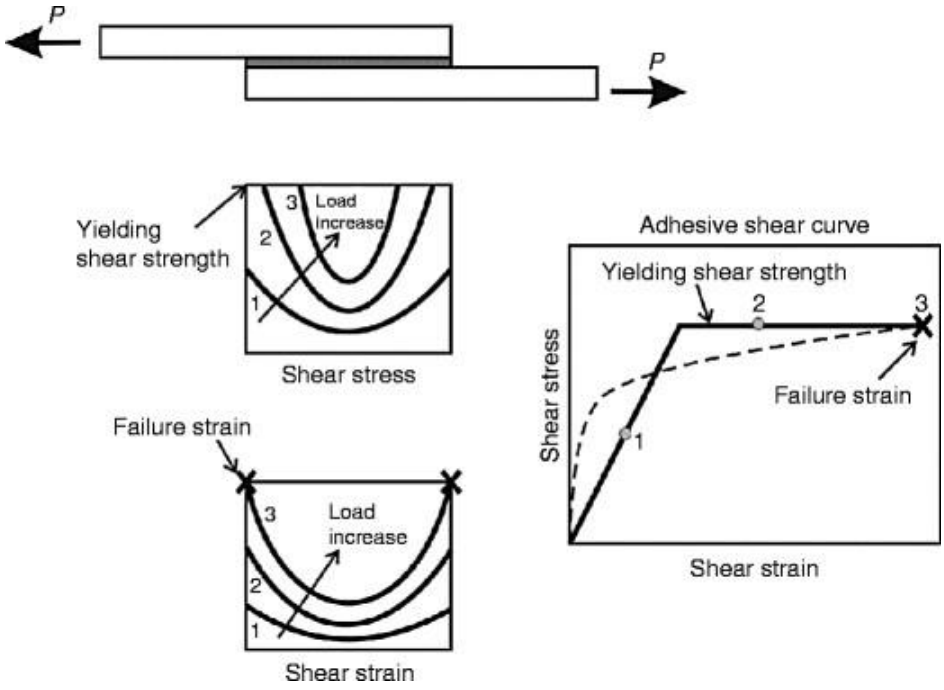

Figure 14 - Hart-Smith analysis [21].

Renton and Vinson [22] made another significant contribution to the analysis of SLJ. They used balanced SLJ boundary conditions based on Goland and Reissner's formulation for the overlap bending moment, but they included thermal strains in the formulation and the adhesive layer was modelled as a separate block. This enables the adhesive shear stress to drop rapidly to zero at the overlap edges.

Ojalvo and Eidinoff [23] incorporated a complete description for the adhesive shear strain that allows for a linear variation across the adhesive thickness. Substrate shearing has not been included. The authors showed that shear stresses could exhibit a significant variation across the overlap at the joint ends.

Allman [24] and Chen and Cheng [25], using models based on the two dimensions (2D) elastic theory, assumed a linear variation of peel stresses and constant shear stresses across the adhesive thickness. Adams and Mallick [26], and then Zhao and Lu [27], developed models in which both the adhesive and adherends are described as elastic media. Their models can be applied in joints with thick adhesives, although analytical solutions of composite joints are too complicated with this model [21].

Yang and Pang [28] further developed a model for SLJ including asymmetric laminates, and all three stress components in the adhesive were obtained through a Fourier series approach.

Several authors developed other methods to establish strength prediction of SLJ as well as other joint configurations. To provide design analysis for a wide range of structures, capable of modelling non-linear adhesive behaviour, general structural analysis packages were developed. These analyses were restricted to just one overlap region. Crocombe [29] developed a package known as SAAS (stress analysis for adhesive structures) and, to promote the versatility of the analysis, FE principles were implemented. GLUEMAKER® was another approach to facilitate FE analyses. It is a pre-processor for commercial FE codes such as ABAQUS® [30].

2.3.2. Numerical methods

2.3.2.1. Continuum mechanics

The continuum mechanics approach uses the maximum values of stress, strain or strain energy predicted by an FE analysis or analytical methods and compares them with the corresponding material allowable values to assess failure [31]. Ignoring all the other principal stresses, initially, the maximum principal stress (MAXPS) was used for the strength prediction of brittle materials, because it is the most responsible for the failure of this kind of materials. Adams et al. [32] used this criterion with success. Nonetheless, care must be taken when using this criterion, because of the singularity of stresses at re-entrance corners of the joint. It is known that a small amount of rounding at the adherend corners eliminates the singularity point, and this may affect the stress distributions in that area and also the joint strength. Zhao et al. [33, 34] studied the effect of adherend rounding (Figure 15) and showed that the stress singularity became null with a small degree of rounding, as presented in Figure 16.

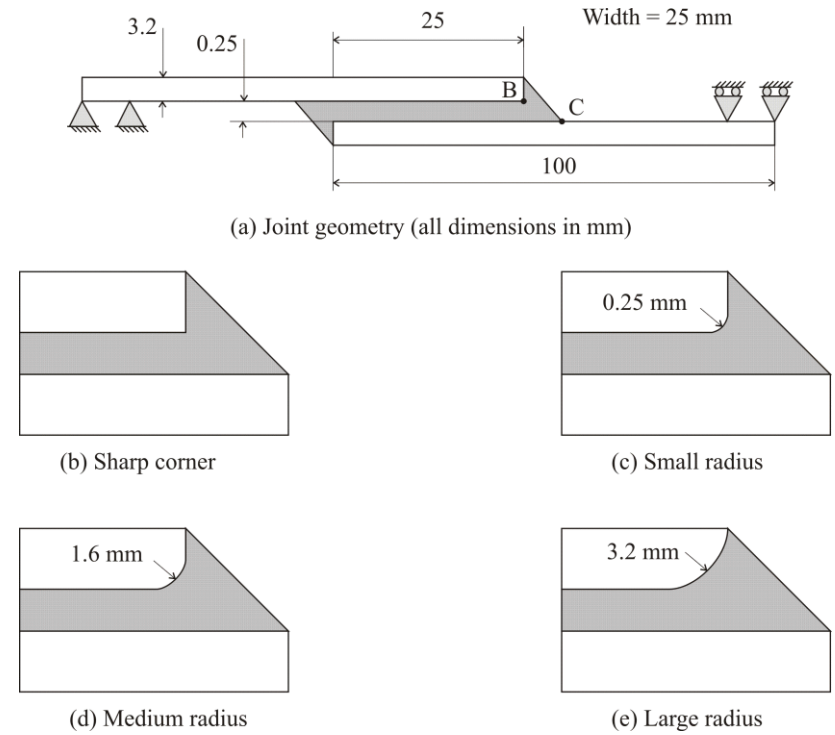

Figure 15 - SLJ with different degrees of rounding [33]

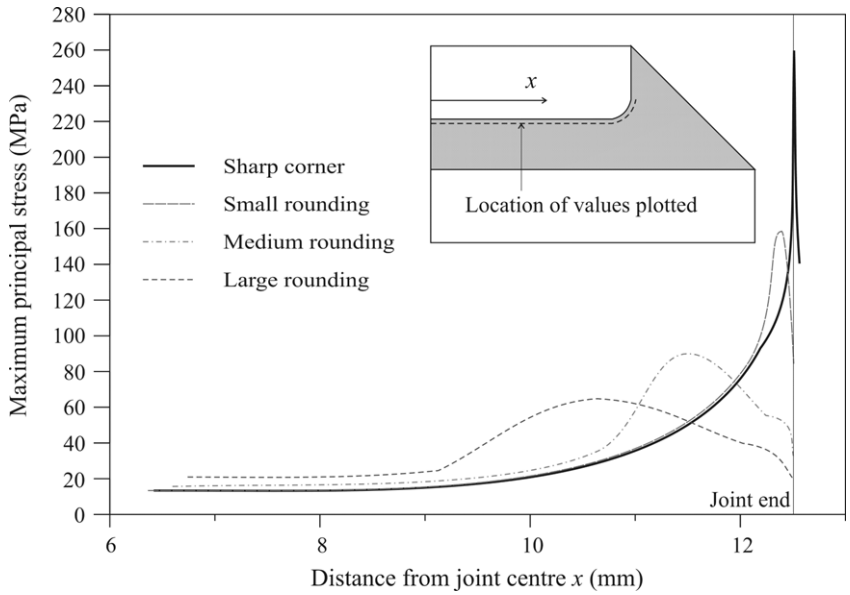

Figure 16 - Maximum principal stresses in the adhesive close to the unloaded adherend [33]

Shear stresses have also been used for strength prediction. da Silva et al. [17, 35] showed for SLJ that this criterion is only valid for brittle adhesives and short overlaps. For ductile adhesives, which can endure large loads after adhesive yielding, the criterion of maximum principal strain (MAXPE) can be used. However, as well as the maximum principal stresses, this criterion is sensitive to mesh the size. Hart-Smith [20] proposed that the maximum shear strain might be used as a failure criterion when plastic deformation was apparent. da Silva et al. [17, 35] showed, for SLJ, that the maximum shear strain criterion is very accurate for ductile adhesives. The above-mentioned criteria are applicable to continuous structures only.

2.3.2.2. Fracture mechanics

Continuum mechanics assumes that the structure and its materials are continuous. However, defects in structures or two materials with re-entrant corners constitute a structural discontinuity. Continuum mechanics gives no solution for these cases. Therefore, fracture mechanics has been developed. With this approach, it is well accepted that stresses calculated by using continuum mechanics are singular at the crack tip. Figure 17 helps to explain why these singularities exists.

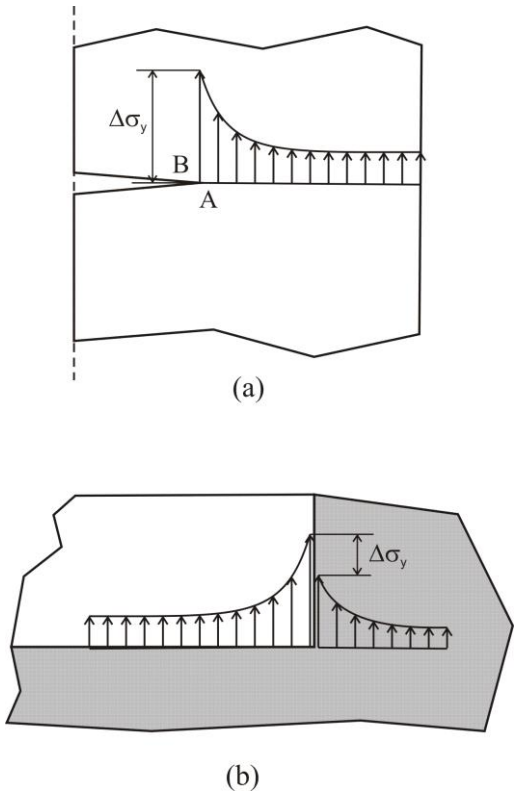

Figure 17 - Stress discontinuity around (a) a crack tip and (b) at a re-entrant corner [31]

The normal y-stresses, σ_y, must be finite, instead of infinite as theory predicts. However, σ_y stresses into the crack and away from the tip of the crack are null because of the free surfaces. Therefore, a discontinuity exists at point A. The continuum mechanics criterion requires all the stresses to be continuous, fact that is not observed at the crack tip. As a result, stresses at the crack tip must be finite, instead of infinite (as theory predicts). Williams [36] found that a singularity always exists when the crack angle is < 180°. Actually, the stress discontinuity still exists, but free surfaces do not [31]. Fernlund and Spelt [37] and Shahin and Taheri [38], among others, used the strain energy release rate, G, and respective critical value or fracture toughness, G_C, instead of stress intensity factors. However, fracture of adhesive joints typically takes place under mixed-mode. Failure criteria for mixed mode fracture can be developed similarly to the classical failure criteria, although the mixed-mode loadings oblige to take into account the toughness in tension (G_{Ic}) and toughness in shear (G_{IIc}). Failure criteria for mixed-mode fracture can be developed in a way analogous to the classical failure criteria, although the fracture surface (or envelope) concept must be introduced. Various mathematical surface functions were proposed such as the 3D criterion by Dillard et al. [39]

$$\left(\frac{G_I}{G_{IC}}\right)^{\alpha}+\left(\frac{G_{II}}{G_{IIC}}\right)^{\beta}+\left(\frac{G_{III}}{G_{IIIC}}\right)^{\gamma}=1, \quad (1)$$

where G_I, G_{II} and G_{III} are the values of G under pure tension, shear and tearing modes, respectively, and G_{IC}, G_{IIC} and G_{IIIC} are the respective critical values. The linear energetic criterion (α=β=γ=1) and the quadratic energetic criterion (α=β=γ=2) are the most used. Constructing such envelopes involves fitting with experiments, or assuming a pre-established shapes, although the fitting method does not help much to understand the physical failure mechanism of mixed mode fractures. When materials deform plastically, the linear elastic fracture mechanics (LEFM) concepts have to be extended into elasto-plastic fracture mechanics. Rice and Rosengren [40] proposed the *J*-integral to solve those problems. The *J*-integral has been successfully used by researchers to predict the joint strength of cracked adhesive joints

$$J=\int_c w dx_2 - T_j \frac{\partial u_j}{\partial x_1} dS, \quad (2)$$

where *C* is the curve surrounding the crack tip, *S* indicates the arc length, *W* the energy density, T_j is the traction vector, u_j the displacement vector and x_1 –x_2 is the coordinate system. However, this approach may not be used as a strength criterion for joints without a pre-crack [31].

2.3.2.3. Cohesive zone models

The computer implementation of LEFM techniques had a great success some decades ago, but these are limited to the elastic behaviour of materials. Moreover, modern toughened adhesives usually develop plastic zones larger than the adherends' thickness, which requires a proper technique to overcome this problem. Barenblatt [41, 42] and Dugdale [43] proposed the concept of cohesive zone to describe damage under static load at the cohesive process zone ahead of the apparent crack tip. Since then, CZM were improved and tested to simulate crack initiation and propagation even in composite delamination [44]. CZM are based on spring [45] or more typically cohesive elements [46], connecting 2D or 3D elements of structures. CZM can be easily incorporated in FE software to model the fracture behaviour in various materials. CZM are based on the assumption that a fracture can be artificially introduced in structures, in which damage growth is allowed by the introduction of a possible discontinuity in the displacement field. This technique consists of the establishment of traction-separation laws to model interfaces or finite regions.

CZM reproduce the damage along a given path, disregarding the phenomena on the origin of failure establishing a traction-relative displacement (t-δ), by specification of several parameters ruling the crack growth process such as G_{IC}, G_{IIC} or G_{IIIC} [34]. The traction-separation laws are typically represented by linear relations at each one of the loading stages [47]. Figure 18 presents the 2D triangular CZM model implemented in Abaqus® for static damage growth in pure and mixed mode.

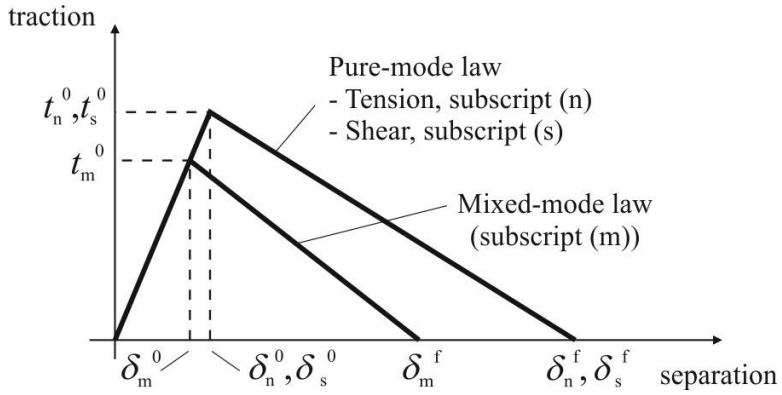

Figure 18 - Triangular traction-separation law (adapted from Abaqus® [48])

The subscripts *s* and *n* relate to pure normal (tension) and shear behaviours, respectively. t_n and t_s are the corresponding current stresses, and δ_n and δ_s the current values of δ. G_I and G_{II} along the fractures path and respective values of G_{IC} and G_{IIC} are required. The cohesive strengths must be defined (t_n^0 for tension and t_s^0 for shear), cancelling the elastic behaviour and leading to the initiation of stress softening. δ_n^0 and δ_s^0 are the peak strength displacements, and δ_n^f and δ_s^f the failure displacements. For the mixed-mode model, t_m^0 is the mixed-mode cohesive strength, δ_m^0 the corresponding displacement, and δ_m^f the mixed-mode failure displacement. Under pure-mode loading, the damage initiation occurs at the cohesive strength (t_n^0 or t_s^0) and, when the values of *t* became null, the crack propagates up to the adjacent pair of nodes in the failure path allowing the gradual debonding between crack surfaces. Under mixed-mode loading, stress and/or energetic criteria are often used to combine the pure-mode laws. Through those principles, the complete failure response of structures may be simulated [49]. CZM has more utility than conventional fracture mechanics, as it does not need an initial flaw. CZM extends the concepts of continuous mechanics by including a zone of discontinuity by means of a CZM path. CZM has been used to simulate the behaviour of structures up to failure. The knowledge of the spot where damage will start is not necessary, although cohesive elements must exist at the planes where damage could occur, which in some cases is not easy to know beforehand. However, an important feature of adhesively bonded joints, that helps to overcome the issue, is that damage propagation is restricted to well defined plans (at or near the adhesive/adherend interfaces, or cohesively in the adhesive bond) [50].

2.3.3. Cohesive law shapes

Over the years several models were developed include triangular [51], linear-parabolic [52], polynomial [53], exponential [54] and trapezoidal laws [55]. In order to faithfully simulate the behaviour of thin material strips or interfaces, the shape of CZM laws can be adjusted. Figure 19 presents those CZM models used for strength prediction of different materials.

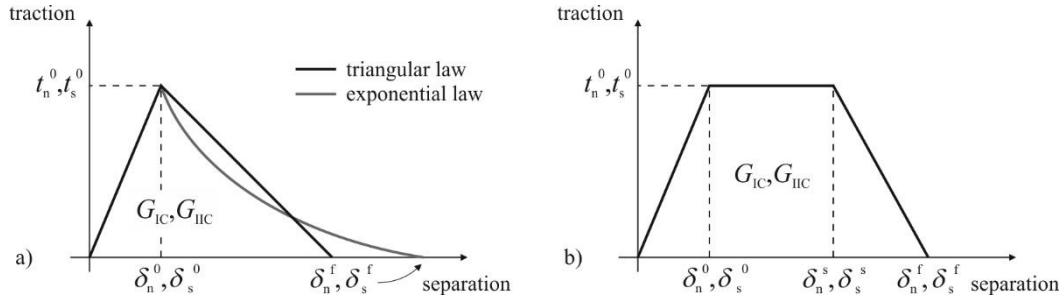

Figure 19 - Different shapes of pure mode CZM laws: triangular or exponential (a) and trapezoidal (b)

For the represented trapezoidal CZM, δ_n^s and δ_s^s are the stress softening onset displacements. Campilho et al. [50, 56], in order to simulate ductile adhesives, considered trapezoidal softening laws. Other study from Pinto et al. [57] concluded that, for stiffer adherends, a precise shape of the cohesive law is fundamental for the accuracy of the results and *P-δ* response of the structure and also that the *P-δ* curve precisely follows the shape of CZM law.

At a glance, the trapezoidal law is often preferred for ductile adhesives [46, 58] and a triangular CZM is normally used for brittle materials that do not plasticize before failure [59]. The material behaviour should always be the main factor for the choice of the most appropriate CZM law shape.

2.3.3.1. Damage mechanics

In these methods, a damage parameter is established to modify the constitutive response of materials through a decreasing of stiffness or strength to represent the severity of damage material during loading. Literature examples that used properties degradation are found in thin adhesive bonds [60], composite delaminations or matrix failure [61]. This parameter can be used in a damage evolution law to model pre-cracking damage and crack growth. The damage variables can be categorized in two main groups, one that predicts the amount damage by redefinition of the material constitutive properties, and other considering variables linked to a specific kind of damage, such as porosities [62]. By damage mechanics techniques the growth of damage is defined as a function of the load for static modelling [63] or cycling count for fatigue analyses [64]. Compared to fatigue CZM, damage mechanics techniques do not provide a clear distinction between fatigue initiation and propagation phases [60]. Nonetheless, these may be recommended if the damage is more widespread or the failure path is not known [65]. A few works currently exist in the field of static applications of damage mechanics [66, 67]. The work of Sampaio et al. [68], addressed damage behaviour of an adhesive joint by an analytical damage mechanics model accounting for the value of t_A. The authors observed that comparing the predicted values of failure stress against experimental data for different values of t_A, a good agreement was found. Hua et al. [69] proposed a mesh-independent damage mechanics model to predict the residual strength of adhesively bonded joints with the ductile adhesive Hysol® EA9321 under different scenarios of environmental degradation. The study was performed by introducing a displacement-based damage parameter into the constitutive equation of damage materials, which allowed to establish a linear response of the material behaviour. The mesh independency derived from a damage parameter that is defined in terms of the equivalent plastic displacement rather than strain. The study concluded that the joint strength predictions and the respective damage initiation and propagation during loading matched well with the experimental data. This technique was considered as useful to predict the

environmental degradation, the failure path and the actual degree of damage in ductile bonded joints, where failure is predominantly within the adhesive bond.

2.3.3.2. Extended finite element method

The recently developed eXtended Finite Element Method (XFEM) is an extension of the FE method and its fundamental features were firstly presented in the late 1990s by Belytschko and Black [70]. This method, contrary to CZM, does not require the crack to follow a predefined path. XFEM simulates crack onset and growth along an arbitrary path without the requirement of the mesh to match the geometry of the discontinuities neither remeshing near the crack [71]. It is based on concept of partition of unit, which consists on the introduction of local enrichment functions for the nodal displacements to model crack growth and separation between crack faces [72]. As the crack tip grows, it continuously changes its position and orientation due to loading conditions, and the XFEM algorithm creates the necessary enrichment functions for the nodal points of the FE around the crack path/tip. XFEM uses damage laws based on the bulk strength of the materials for the initiation of damage and strain for the assessment of failure (defined by G_{IC}), rather than values of t_n^0/t_s^0 or δ_n^0/δ_s^0 used in CZM. Therefore, damage and failure are simulated by suitable damage initiation criteria (MAXPS and MAXPE) and damage laws (traction-separation laws that simulate material degradation up to failure) between the real and phantom nodes of a cracked element. In the presence of damage propagation, phantom nodes are established that subdivide elements cut by a crack and simulate separation between the newly created sub elements. Initially, phantom nodes have the same coordinates than the real nodes and are completely constrained to the real nodes up to damage initiation.

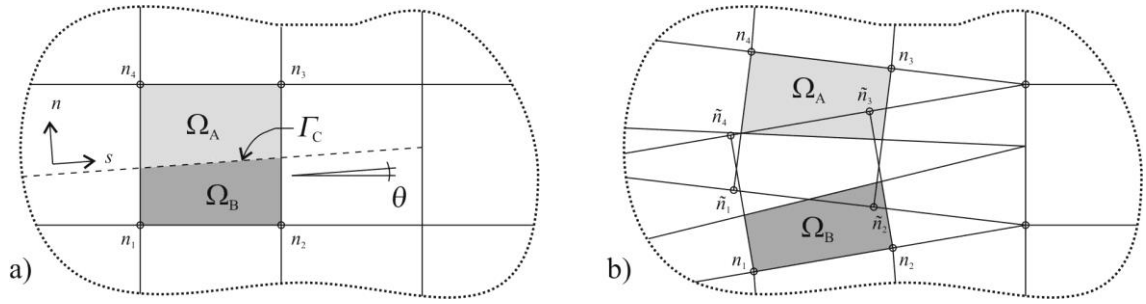

Figure 20 - Damage propagation using the phantom nodes concept: before (a) and after partitioning (b) of a cracked element into sub-elements [73]

In Figure 20, the highlighted element has nodes n_1-n_4. After being crossed by a crack, the element is divided in two sub-elements. The discontinuity in the displacements is made possible by adding phantom nodes ($\tilde{n}_1$-$\tilde{n}_4$) superimposed to the original nodes. When an element cracks, each one of the two sub-elements will be formed by real nodes (the ones corresponding to the cracked part) and phantom nodes (the ones that no longer belong to the respective part of the original element). These two elements that have fully independent displacement fields replace the original one. From this point, each pair of real/phantom node of the cracked element can separate according to a suitable cohesive law up to failure. If initiation criteria are based on principal stresses or strains,

crack initiation/propagation will always take place orthogonally to the maximum principal stresses or strains.

Several applications to this innovative technique were proposed to simulate different engineering problems. In 2000, three-dimensional damage simulations [74] and modelling cracks with multiple branches, multiple holes and cracks emanating from holes [75] were made available. In 2002, Moës and Belytschko [76] solved the problem of cohesive propagation of cracks in concrete structures considering three-point bending and four point shear scaled specimens. The use of plastic enrichments in XFEM modelling to capture the singular fields in elasto-plastic fracture mechanics was proposed by Elguedj et al. [77]. Campilho et al. [59] predicted the strength of single and double lap joints made of aluminium adherends and bonded with a brittle adhesive (Araldite® AV138) by standard FEM and XFEM. It was shown that, due to the direction of crack growth being ruled by the maximum principal stresses/strains at the crack tip, the damage grows towards and within the adherends, which is not consistent with the real behaviour of the joints. However, the XFEM was used with satisfactory results to predict failure by approximating it to damage onset at the overlap edges. However, results were mesh dependent.

3. MATERIALS AND METHODS

This section describes the materials used in the experimental and numerical parts of this work. It should be noted that the experimental work was carried out in a previous work [78], which is described in this work in a simplified manner.

3.1. Materials

The next subsections concern the materials used to perform the experimental work, and their most relevant mechanical properties useful for the experimental and numerical analyses.

3.1.1. Adherends

The material used as adherend in all joints was the high strength and ductile aluminium alloy AW6082-T651. This alloy is obtained through artificial ageing at 180°C [79], and it was selected not only because of its good mechanical properties, but also due to the vast structural applications under different extruded or rolled shapes. This aluminium alloy was characterized in the work of Campilho et al. [59], where the most relevant mechanical properties presented in Table 1 were defined.

Table 1 - Relevant mechanical properties of the aluminium alloy AW6082-T651 [59]

Properties	Aluminium 6082-T651
Tensile failure stress, σ_f [MPa]	324.00±0.16
Young´s modulus, E [GPa]	70.07±0.83
Tensile yield stress, σ_y [MPa]	261.67±7.65
Tensile Failure strain, ε_f [%]	21.70±4.24
Poisson´s ratio, v	0.3*

* Manufacturer´s value

The aluminium σ-ε curves presented in Figure 21 were experimentally obtained according to the ASTM-E8M-04 standard [59]. The numerical approximation used in the numerical simulations is also represented.

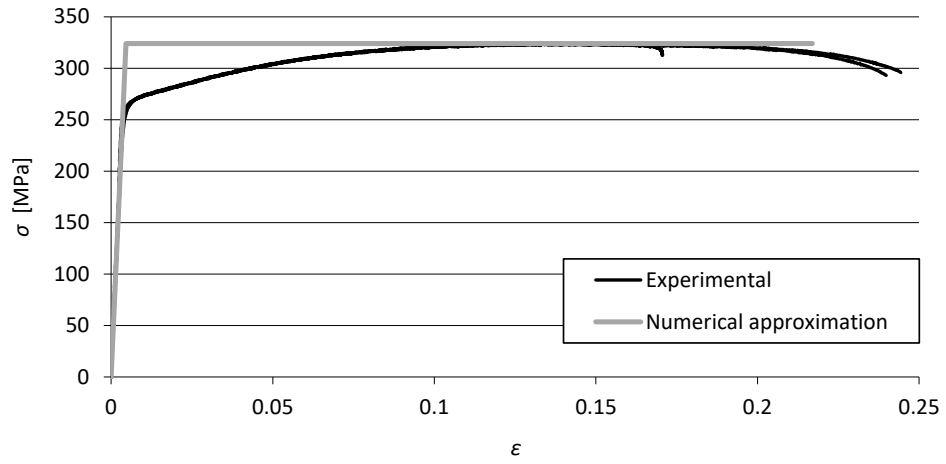

Figure 21 - Aluminium σ-ε curves and numerical approximation [59]

3.1.2. Adhesives

The three tested adhesives were all two-part (resin + hardener), two epoxy (Araldite® AV138 and Araldite® 2015) and one polyurethane (Sikaforce® 7752). They all present a low viscosity, which promotes an easier application on the adherends.

3.1.2.1. Araldite® AV138

The structural epoxy adhesive Araldite® AV138 is manufactured by HUNTSMAN ADVANCED MATERIALS. It has a brittle behaviour but high strength (Figure 22, Table 2), and it is suitable to join miscellaneous materials like metals, composites, polymers [80].

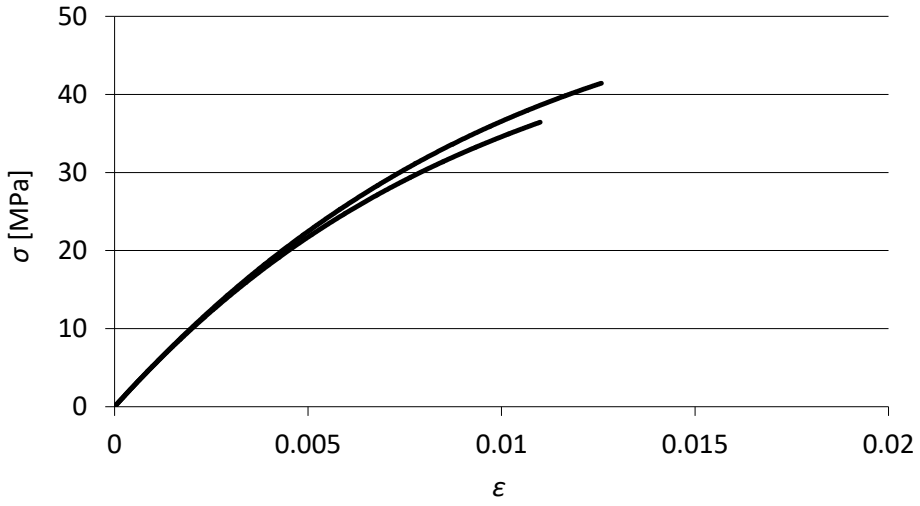

Figure 22 - σ-ε curves estimated by the bulk specimens of the Adhesive Araldite® AV138 [59]

This adhesive is provided in two recipients (Figure 23), one with a thermoset resin AV138 and other with the hardener HV998, and the mixture is performed manually after weighting in the correct proportion. The mixture proportion is 100 g of resin for 40 g of hardener, with an accuracy of ±5%.

This adhesive is a thixotropic gap filling paste with low out gassing and volatile loss, and it cures at temperatures down to 5°C.

Figure 23 - Adhesive Araldite® AV138 [81]

Table 2 - Properties of the Araldite® AV138 [82]

Properties	Araldite® AV138
Young´s modulus, E [GPa]	4.89±0.81
Poisson´s ratio, v	0.35*
Tensile yield stress, σ_y [MPa]	36.49±2.47
Tensile failure stress, σ_f [MPa]	39.45±3.18
Tensile failure strain, ε_f [%]	1.21±0.10
Shear modulus, G [GPa]	1.56±0.01
Shear yield strength, τ_y [MPa]	25.10±0.33
Shear failure strength, τ_f [MPa]	30.20±0.40
Shear failure strain, γ_f [%]	7.80±0.70
Toughness in tension, G_{Ic} [N/mm]	0.20**
Toughness in shear, G_{IIc} [N/mm]	0.38**
Glass transition temperature, T_g [°C]	66

* - Manufacturer´s value

** - Estimated in reference [59].

3.1.2.2. Araldite® 2015

The adhesive Araldite® 2015 is also manufactured by Huntsman Advanced Materials, and it is equally a two-part structural epoxy adhesive. It shows a smaller ultimate strength than the previous adhesive and has intermediate ductility, allowing large plastic flow prior to failure. A redistribution of stresses occurs at stress concentrated regions which usually take place in the edges of the overlap ends of bonded joints. Figure 24 shows the cartridges incorporating mixers for application of the adhesive.

Figure 24 - Adhesive Araldite® 2015 [81]

The bond strength and durability of joints with this adhesive are dependent on an adequate surface treatment. At least, surfaces to be bonded should be clean with solvent wiping (acetone). However, surface preparation may also include a combination of mechanical abrading, chemical cleaning and acid etching [83].

The analysis of Figure 25 and Table 3, which present the σ-ε curves and mechanical properties, respectively, shows that the shear failure strain is six times higher than that of the previous adhesive. However, the tensile and shear failure strength of the Araldite® AV138 is twice the value of the Araldite® 2015. Thus, this ductile adhesive allow stress distribution at the stress concentration area, typically at the edges of the overlap due to joint asymmetry and to the adherends' differential deformation [84].

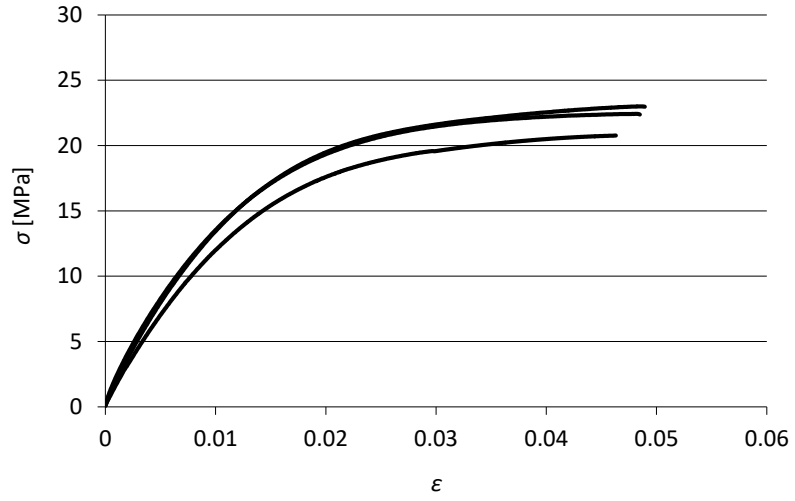

Figure 25 - σ-ε curves estimated by the bulk specimens of the Araldite® 2015 [85]

Table 3 - Properties of the Araldite® 2015 [85]

Properties	Araldite® 2015
Young´s modulus, E [GPa]	1.85±0.21
Poisson´s ratio, v	0.33*
Tensile yield strength, σ_y [MPa]	12.63±0.61
Tensile failure strength, σ_f [MPa]	21.63±1.61
Tensile failure strain, ε_f [%]	4.77±0.15
Shear modulus, G [GPa]	0.56±0.21
Shear yield strength, τ_y [MPa]	14.60±1.3
Shear failure strength, τ_f [MPa]	17.9±1.8
Shear failure strain, γ_f [%]	43.9±3.4
Toughness in tension, G_{Ic} [N/mm]	0.43±0.02
Toughness in shear G_{IIc} [N/mm]	4.70±0.34
Glass transition temperature, T_g [°C]	87

* - Manufacturer´s value

3.1.2.3. Sikaforce® 7752

The structural polyurethane adhesive Sikaforce® 7752 is manufactured by Sika® and it is provided in two parts (Figure 26). The mixing proportion is 100 g of resin for 20 g of hardener.

Figure 26 - Adhesive Sikaforce® 7752 [86]

It is the most ductile of the three adhesives, as depicted in the σ-ε curves of Figure 27. Analysing the mechanical properties presented in Table 4, the adhesive Sikaforce® 7752 has the lowest tensile

and shear tensile strength. However, it has high ductility, which allows large plastic flow prior to failure, resulting in a higher joint strength [87].

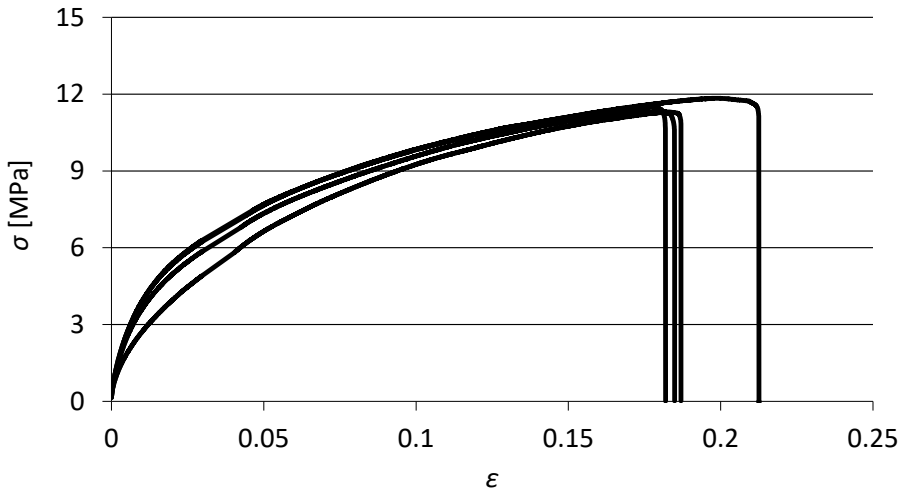

Figure 27 - σ-ε curves estimated by the bulk specimens of the Sikaforce® 7752 [87]

Table 4 - Properties of the Sikaforce® 7752 [87]

Properties	Sikaforce® 7752
Young´s modulus, E [GPa]	0.49±0.09
Poisson´s ratio, v	0.30*
Tensile yield strength, σ_y [MPa]	3.24±0.48
Tensile failure strength, σ_f [MPa]	11.48±0.25
Tensile failure strain, ε_f [%]	19.18±1.40
Shear modulus, G [GPa]	0.19±0.01
Shear yield strength, τ_y [MPa]	5.16±1.14
Shear failure strength, τ_f [MPa]	10.17±0.64
Shear failure strain, γ_f [%]	54.82±6.38
Toughness in tension, G_{Ic} [N/mm]	2.36±0.17
Toughness in shear G_{IIc} [N/mm]	5.41±0.47
Glass transition temperature, T_g [°C]	Not Available

* Manufacturer´s value

3.2. Geometry and dimensions of the joint

The joints' geometry follows the representation in Figure 28.

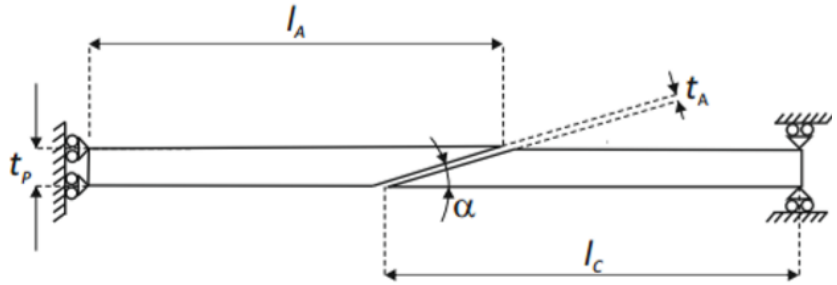

Figure 28 - Scarf Joint Geometry

The variables are presented in Table 5. These represent the joint's dimensions. All the scarf joints have the same general dimensions, like length, width, and thickness (substrate and adhesive). The variable, in this case, is the chamfer angle, along with temperature and adhesive type.

Table 5 - Adhesive joints' dimensions.

Aluminium substrate length, l_A [mm]	100
Test specimen's useful length, l_0 [mm]	200
Width, w [mm]	25
Test specimen's thickness, t_P [mm]	3
Adhesive's thickness, t_A [mm]	0.2
Chamfer angle, α [°]	3.43; 10; 15; 20; 30; 45

3.2.1. Joints' strength

In this subchapter, two tables are presented that allow the comparison between the adhesives, SJ angles and ΔTs, with max P values.

Table 6 - P_{max} values (in N) obtained in function of adhesive, α and ΔT.

	ΔT/α	3.43°	10°	15°	20°	30°	45°
Araldite® 2015	0	20808.119	7172.509	4865.886	3725.265	2604.605	1948.024
	40	20808.193	7171.240	4865.861	3726.146	2604.349	1947.976
	80	20806.551	7185.644	4833.027	3726.222	2604.297	1947.839
Araldite® AV138	0	30775.334	11221.544	7846.778	6106.856	4308.900	3301.143
	40	30774.924	11221.282	7846.792	6106.715	4308.575	3300.862
	80	30778.115	11220.963	7846.810	6106.522	4308.307	3300.484
Sikaforce® 7752	0	11855.332	4081.059	2758.745	2108.839	1460.563	1077.122
	40	11862.695	4087.275	2758.525	2101.570	1458.599	1077.120
	80	11849.387	4085.548	2760.947	2106.141	1462.052	1077.010

From the analysis of the data in Table 6,

- Temperature does not affect P_{max};
- α significantly influences P_{max} as the smaller angle has the highest results;
- AV138 has P_{max} values superior than 2015, which in turn is higher than 7752.

Table 7 - Displacement (in mm) at P_{max} values obtained in function of adhesive, α and ΔT.

	ΔT/α	3.43°	10°	15°	20°	30°	45°
Araldite® 2015	0	0.772	0.285	0.201	0.160	0.119	0.091
	40	1.006	0.517	0.435	0.394	0.353	0.325
	80	1.241	0.752	0.671	0.629	0.587	0.559
Araldite® AV138	0	1.106	0.408	0.289	0.228	0.165	0.128
	40	1.340	0.642	0.523	0.462	0.399	0.362
	80	1.575	0.876	0.758	0.696	0.634	0.596
Sikaforce® 7752	0	0.475	0.200	0.150	0.125	0.100	0.077
	40	0.711	0.433	0.384	0.362	0.336	0.311
	80	0.943	0.668	0.618	0.595	0.568	0.546

However, in Table 7,

- as ΔT increases, displacement in which P_{max} is achieve increases because there's displacement that occurs before P starts to increase;
- α has the same effect in displacement as it has in P_{max};
- the same applies to the adhesives.

3.3. Preparation of numerical models

For the numerical analysis, the 2017 version of Abaqus® software was selected. The FEM based software with a CZM integrated module is capable of evaluate damage simulation and strength prediction, under thermal loading.

The joints were modelled in 2D, using solid elements with a plane state of elements to model the adherents (CPE4R and CPE3). The adhesive layer was modelled by a row of cohesive elements with 0.1 x 0.2 mm, in the thickness direction and a triangular traction-separation law that includes the stiffness of the adhesive layer.

A model is created with the properties as described in 3.1 and the dimensions of 3.2 (Figure 29). In the module "Part", the outer limits are dimensioned and the model is divided in sections to create the scarf geometry and both adhesive and interlaminar layers.

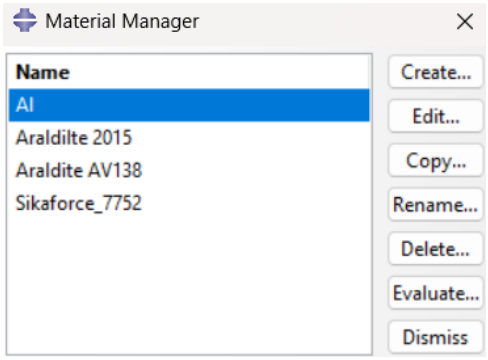

Figure 29 - Materials and properties to select.

Besides the common mechanical properties such as Youngs' modulus, Poisson's ratio and density, it is also necessary to introduce thermal expansion coefficients and thermal conductivity. The model is in mm, therefore, the scaling factor was applied with precaution.

In this study, the "static general" models already existed from a previous work, as cohesive zone modelling. Firstly, the step was replaced by "coupled temperature-displacement". All steps must be like this due to the nature of the study where there are temperatures, heat fluxes and other thermal variables. There were also configured as "Steady-State" because a correlation between temperature and time is not needed ("transient"). And then, there was an introduction of a "Heat" step. Therefore, the model has two steps that represent heating and pulling. There's an introduction of temperature according to the defined parameters followed by a simulation where the joint is pulled apart like in a UTM test.

After that, like a mechanical analysis, a "Field of Temperature" is added, however, only to the adherends, since cohesive elements cannot conduct heat, in the initial step. The reference temperature is 20 °C.

In the meshing process, the elements have a temperature degree of freedom and as mentioned the element type was changed to a "coupled temperature-displacement" as "plane strain" analysis. However, in the modelling of the adhesive layer with cohesive elements, these elements stay the same (Figure 30).

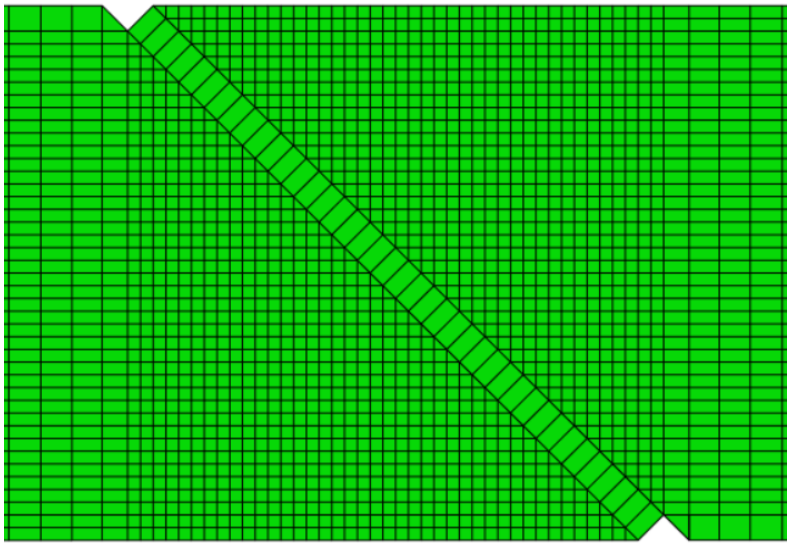

Figure 30 – Meshed SJ model.

Although, cohesive elements cannot transfer heat, these can link to surfaces subjected to temperature changes, therefore, these elements are used to predict joint strength and how the thermal strains induced only by the adherends with affect it. This is present in Abaqus documentation. The material still has an elastic behaviour, and it is modelled as “Traction”.

Afterwards, a quadratic nominal stress damage ('Quads Damage') criterion was added, as well configured for traction. The nominal stresses correspond to the failure stresses in tension, and in shear. Subsequently, the 'Damage Evolution' was added, and the properties correspond to G_{Ic} and G_{IIc}.

The section of the adhesive layer should also be defined as cohesive, when performing a CZM. As the element configuration was already described, the mesh for the adhesive is defined as quadrilateral and sweep. So, the adhesive layer’s mesh was defined first, therefore, the element seed of the lines composing the adhesive's interphase should be defined and, after that, for the adhesive thickness (for CZM, it must be of one element).

Figure 31 - Model representation of the boundary and load conditions.

3.4. Cohesive zone model

3.4.1. Triangular damage model

CZM model the elastic loading, initiation of damage and further propagation due to local failure within a material. CZM are based on a relationship between stresses and relative displacements connecting initially superimposed nodes of the cohesive elements (Figure 18), to simulate the elastic behaviour up to a peak load and subsequent softening, to model the gradual degradation of material properties up to complete failure. Generically speaking, the shape of the softening laws can be adjusted to conform to the behaviour of the material or interface they are simulating [50, 56]. The areas under the traction-separation laws in each mode of loading (tension and shear) are equalled to the respective fracture energy. Under pure mode, damage propagation occurs at a specific integration point when the stresses are released in the respective traction-separation law. Under mixed-mode, energetic criteria are often used to combine tension and shear [50], thus simulating the typical-mixed mode behaviour inherent to bonded assemblies. In this work, a continuum-based approach, i.e., using the cohesive elements to model solids rather interfaces, was considered to model the finite thickness of the adhesive layer. The cohesive layer is assumed to be under one direct component of strain (through-thickness) and one transverse shear strain, which are computed directly from the element kinematics. The membrane strains are assumed as zero, which is appropriate for thin and compliant layers between stiff adherends. The strength predictions of CZM modelling are expected to be mesh independent [59].

The traction-separation law assumes an initial linear elastic behaviour followed by linear evolution of damage. Elasticity is defined by an elastic constitutive matrix relating stresses and strains across the interface [48]

$$\mathbf{t} = \begin{Bmatrix} t_n \\ t_s \end{Bmatrix} = \begin{bmatrix} K_{nn} & K_{ns} \\ K_{ns} & K_{ss} \end{bmatrix} . \begin{Bmatrix} \varepsilon_n \\ \varepsilon_s \end{Bmatrix} = \mathbf{K\varepsilon}. \quad (3)$$

The stiffness matrix (**K**) contains the stiffness parameters (K_{nn}, K_{ns}, K_{ss}) of the adhesive layer, given by the relevant elastic moduli. A suitable approximation for thin adhesive layers is provided with K_{nn}= E, K_{ss}= G, K_{ns}=0; E and G are the longitudinal and transverse elastic moduli [50]. Damage initiation can be specified by different criteria. In this work, the QUADS criterion was considered for the initiation of damage(equation (4)), already shown to give accurate results [88]. After the peak value in Figure 18 is attained, the material stiffness is degraded under different possible laws, depending on the material to be simulated. For brittle materials such as the Araldite® AV 138, a linear softening law is sufficiently appropriate, Figure 18 [89]. Complete separation is predicted by a linear power law form of the required energies for failure in the pure modes as presented in equation (9), with α=1.

3.4.2. Cohesive parameters' estimate

In order to characterize the tensile and shear cohesive laws, the values of t_n^0, t_s^0, G_{IC} and G_{IIC} are required (Figure 19). Studies were published based on the assumption that, by approximation, those parameters were similar to the ones obtained in experimental bulk adhesives [90, 91]. Nevertheless, the restraint to the adhesive layer's strains due to the adherends vicinity in this type of geometry and the crack propagation under mixed-mode origin a difference between bulk and thin layer adhesive properties [92-94]. Therefore, it becomes necessary to define new methods that provide the adhesive properties adjusted to the geometrical conditions under which they will be employed. The cohesive laws for the Araldite® AV138 were estimated by an inverse method, as presented in the detailed description of Campilho et al. [95]. Due to the non-existence of fracture characterization tests, the tensile and shear strengths obtained by tests with bulk adhesive specimens and thick adherend shear test (TAST) shear test, were used, to estimate t_n^0 e t_s^0, respectively. Those values were used to build an approximate cohesive law, initially using typical G_{IC} and G_{IIC} values for brittle adhesives. The obtained tensile and shear laws were used in the numerical model for one specimen and the adhesive laws were estimated by an adjustment procedure between the numerical and experimental P–δ curves. The obtained G_{IC} and G_{IIC} values were following applied to all joint configurations tested, presenting good results. The E and G values were experimentally estimated by tensile tests to bulk adhesive specimens and TAST tests, respectively. In another work [59], the authors concluded that the obtained parameters simulate the adhesive behaviour with accuracy. Table 8 presents the Araldite® AV138 cohesive parameters used in a mixed-mode cohesive law.

Table 8 - Tensile and shear cohesive parameters for the adhesive Araldite® AV138

E [MPa]	**4890**	**G [MPa]**	**1560**
t_n^0 [MPa]	39.45	**t_s^0 [MPa]**	30.2
G_{IC} [N/mm]	0.2	**G_{IIC} [N/mm]**	0.38

For the adhesive Araldite® 2015, the cohesive laws in the adhesive layer were estimated in previous works [96, 97], through an inverse method to estimate t_n^0 and t_s^0. Although these works present the method with a detailed description, it basically consists of estimating G_{IC} and G_{IIC} through DCB and ENF tests, respectively. G_{IC} or G_{IIC} values are used to build a pure mode cohesive law, in the beginning with an approximate value of t_n^0 or t_s^0, estimated from the known properties of the adhesives. This cohesive law is then used in the correspondent numerical model (DCB for tension or ENF for shear) with the same dimensions as the experimental specimen. The t_n^0 or t_s^0 values are therefore estimated using an adjustment procedure between the numerical and experimental P–δ curves of the respective fracture characterization test, to obtain an approximate behaviour for the adhesive. Table 9 presents the Araldite® 2015 cohesive parameters used in a mixed-mode cohesive law. The E and G values were experimental estimated through bulk and shear tests (TAST), respectively [50].

Table 9 - Tensile and shear cohesive parameters for the adhesive Araldite® 2015

E [MPa]	**1850**	**G [MPa]**	**560**
t_n^0 [MPa]	21.63	t_s^0 [MPa]	17.9
G_{IC} [N/mm]	0.43	**G_{IIC} [N/mm]**	4.70

The cohesive properties of the Sikaforce® 7752 were established in a similar fashion to the Araldite® 2015. Indeed, the shear cohesive law was estimated by an inverse method, obtaining the G_{IIC} value by ENF fracture tests, followed by an iterative manual adjustment to attain t_s^0 [98]. The average values of t_s^0 and G_{IIC} from Azevedo [98] were used, on which deviation between specimens was almost null, showing the repeatability of the performed tests. For the tensile cohesive law, due to the non-existence of an inverse method applied to this adhesive, a different process was performed. G_{IC} was estimated by the average value of DCB fracture tests [99]. The t_n^0 value was approximated to the average value of bulk specimens' tensile strength on the same work [99]. As established in previous works, for the specific case of a tensile loading, t_n^0 has no significant influence on the results for variations until 25% of t_n^0 established by the inverse method (variation for both ways) [99], this procedure was not performed. E and G were experimentally estimated by tensile tests to bulk adhesive specimens and TAST shear tests, respectively [99]. Table 10 presents the cohesive parameters of the Sikaforce® 7752 used in a mixed-mode cohesive law.

Table 10 - Tensile and shear cohesive parameters for the adhesive Sikaforce® 7752

E [MPa]	**493.81**	**G [MPa]**	**187.34**
t_n^0 [MPa]	11.49	**t_s^0 [MPa]**	10.17
G_{IC} [N/mm]	2.36	**G_{IIC} [N/mm]**	5.41

4. RESULTS AND DISCUSSION

4.1. CZM validation

For the comparative experimental work done [78], the substrates were fabricated in AW6082-T651 and the adhesives are the same as the ones in study, Araldite® AV138, Araldite® 2015 and Sikaforce® 7752. There was surface preparation with sanding and acetone cleaning. After that, with bars, clamps, adhesive tape and fishing line (for a constant 0,2 mm gap), adhesive is applied in the substrates and fixed to cure for seven days. Then, all the excess adhesive is removed, and the samples are ready. The traction test was done at RT with clamps, 170 mm apart, at a speed of 1 mm per minute. All samples went to failure.

The comparison between experimental and numerical values of P_{max} (Figure 32), σ at P_{max} (Figure 33) and P-δ curves(Figure 34,Figure 35,Figure 36) was used in the validation of the cohesive laws. The numerical data (Figure 32,Figure 33) of Araldite® AV138 is 1.438% higher in average (range -4.437 to 8.029%) than the experimental. The inverse happens with Araldite® 2015 where the numerical is 1.721% lower in average (range -6.857 to 3.819%). In the case of the Sikaforce® 7752, there is a big discrepancy, the numerical results are 9.864% lower in average.

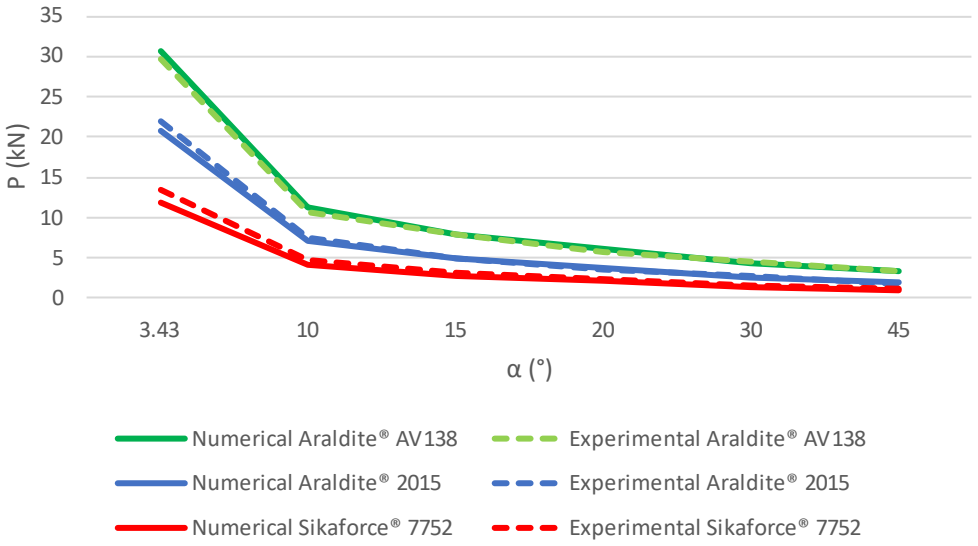

Figure 32 – Comparison between experimental and numerical P_{max} values.

When P_{max} is divided by the area (Figure 33), the difference between the numerical and experimental is more noticeable across the angles in study. There is an oscillation in the adhesives Araldite® AV138 and Araldite® 2015, in contrast to Sikaforce® 7752 where the experimental values are always higher than the numerical ones.

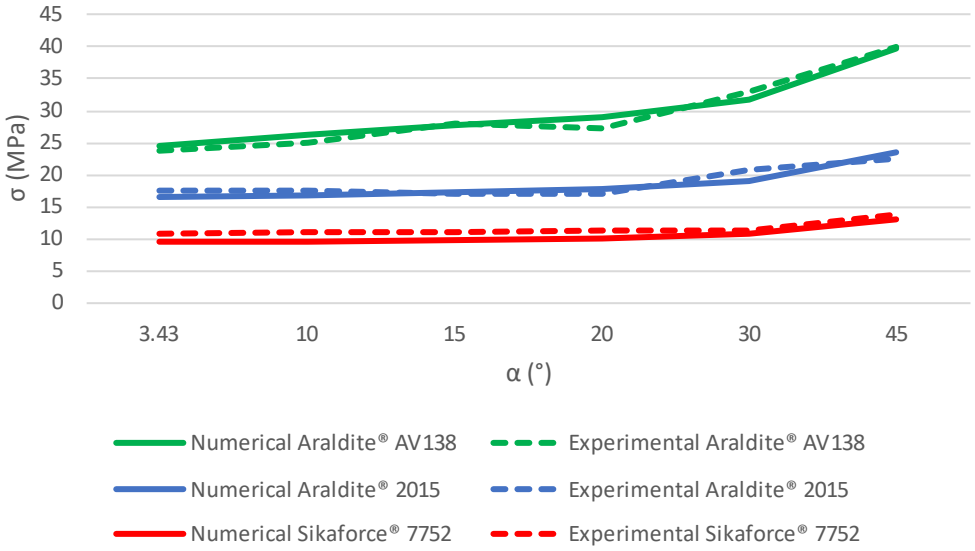

Figure 33 - Comparison between experimental and numerical values of σ at P_{max}.

The most significant difference in value is noticeable in the smaller angle (3.43°). It is also noted that only in Sikaforce® 7752, the difference between the numerical and experimental data gradually decreases as the angle increases.

Table 11 - Numerical P_{max} values (N) by angle in each adhesive for Δt=0.

α (°)	3.43	10	15	20	30	45
Araldite® AV138	30775.334	11221.544	7846.778	6106.856	4308.900	3301.143
Araldite® 2015	20808.119	7172.509	4865.886	3725.265	2604.605	1948.024
Sikaforce® 7752	11855.332	4081.059	2758.745	2108.839	1460.563	1077.122

Table 12 - Average mechanical values of P_{max} (N).

α (°)	3.43	10	15	20	30	45
Araldite® AV138	29700	10648	7926	5715	4480	3325
Standard deviation	1500	346.63	642.49	310.02	150.89	366.66
Araldite® 2015	21903	7509	4858	3567	2832	1868
Standard deviation	1600	772.04	141.92	205.56	101.03	325.56
Sikaforce® 7752	13500	4677	3132	2378	1543	1142
Standard deviation	510.90	195.40	286.25	229.38	167.86	63.51

The numerical P-δ curves for Araldite® AV138 have small differences in comparison with those obtained experimentally. The displacement to P_{max} is generally greater which means that cohesive failure is earlier than the numerical prediction, however, P_{max} values are close, in this case, in between (Figure 32,Figure 34).

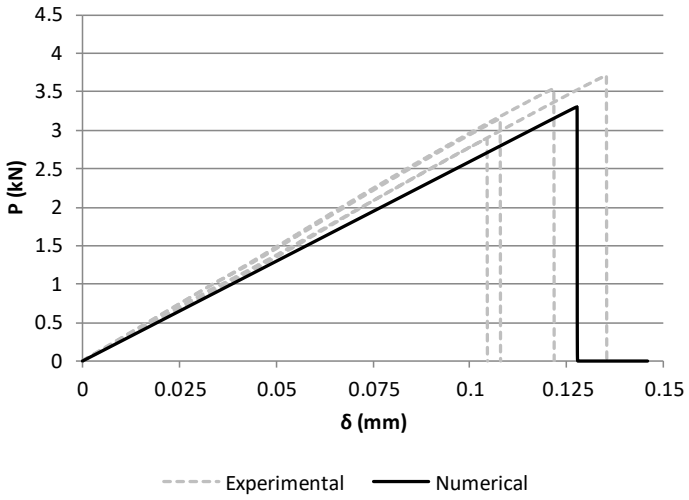

Figure 34 - Comparison between numerical and experimental P-δ curves for Araldite® AV138 at 45°.

In the comparison between numerical and experimental P-δ curves for Araldite® 2015 (Figure 35), it can be observed that P_{max} prediction is below in a couple cases and close with others. This is applicable to the displacement at failure. The biggest differences are in the incline linearity and in the displacement after failure, the moderate ductility in Araldite® 2015 is surprisingly more evident in the numerical analysis.

In the case of Sikaforce® 7752 (Figure 36), the P_{max} prediction is below and displacement at failure is generally below. This is ductile adhesive and, like in Araldite® 2015, the incline linearity is different even after failure.

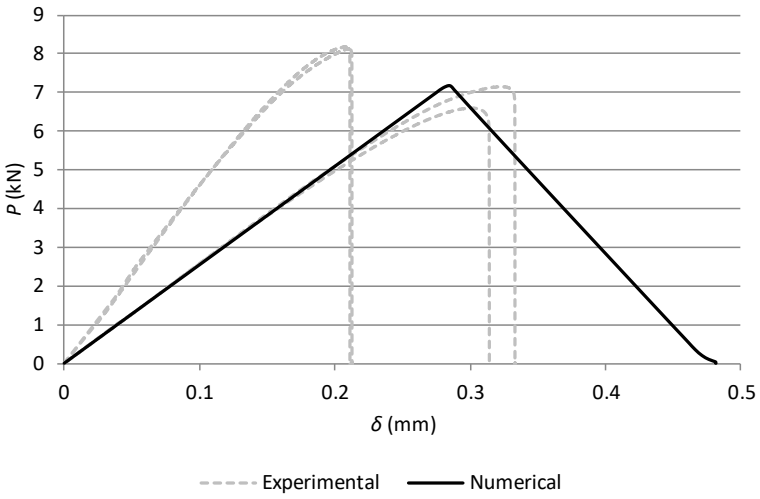

Figure 35 - Comparison between numerical and experimental P-δ curves for Araldite® 2015 at 10°.

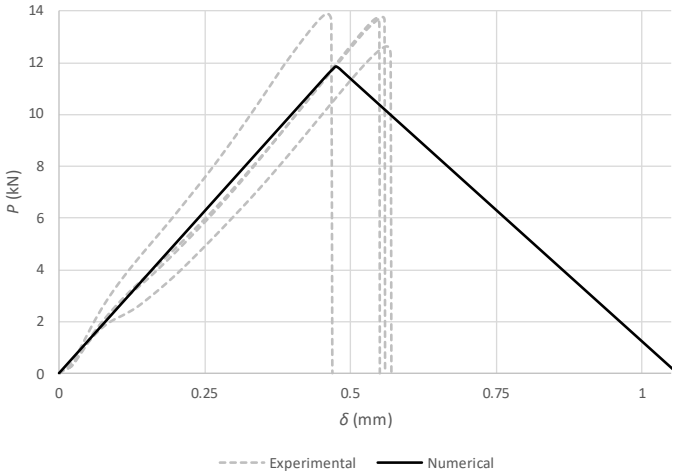

Figure 36 - Comparison between numerical and experimental P-δ curves for Sikaforce® 7752 at 3.43°.

With the analysis of the P-δ curves, there are similar behaviour between Araldite® AV138 and Araldite® 2015 in the framing of P_{max} and displacement at failure with the mechanical results, however, this does not happen at all angles. On the other hand, the numerical prediction of Sikaforce® 7752 is lower at P_{max} and mostly lower in displacement at failure.

4.2. Stress analysis

This analysis is based on the observation of the data extracted from the numerical simulations in ABAQUS ® that was processed in Microsoft Excel® and it is presented in graphics that show stress distribution in the middle of the adhesive layer (x/Lo) between 0 and 1. Both peel and shear stresses are normalized by the average shear stress (τ_{avg}) for every angle and ΔT.

In order to obtain stress distribution and make a comparison between the numerical models, it was considered stress in the middle of the adhesive layer at increment 1 (i.e., identical applied displacement values).

In the analysis of peel stress in function of α at room temperature, σ_y are progressively more uniform with higher averages as α increases, and peak stresses are lower as scarf angle increases (Figure 37). However, the increase in temperature did not change the pattern of stress distribution (Figure 37, Figure 38), nevertheless, peak stresses are higher (Figure 38).

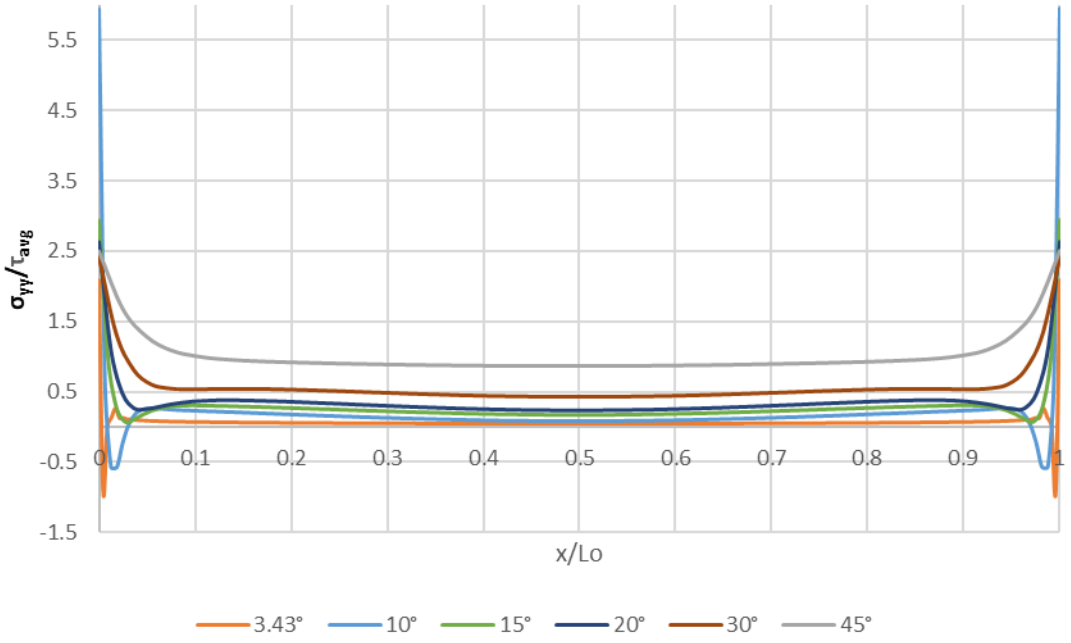

Figure 37 - Comparison of normalised peel stress in Araldite® AV138 across all angles at ΔT=40.

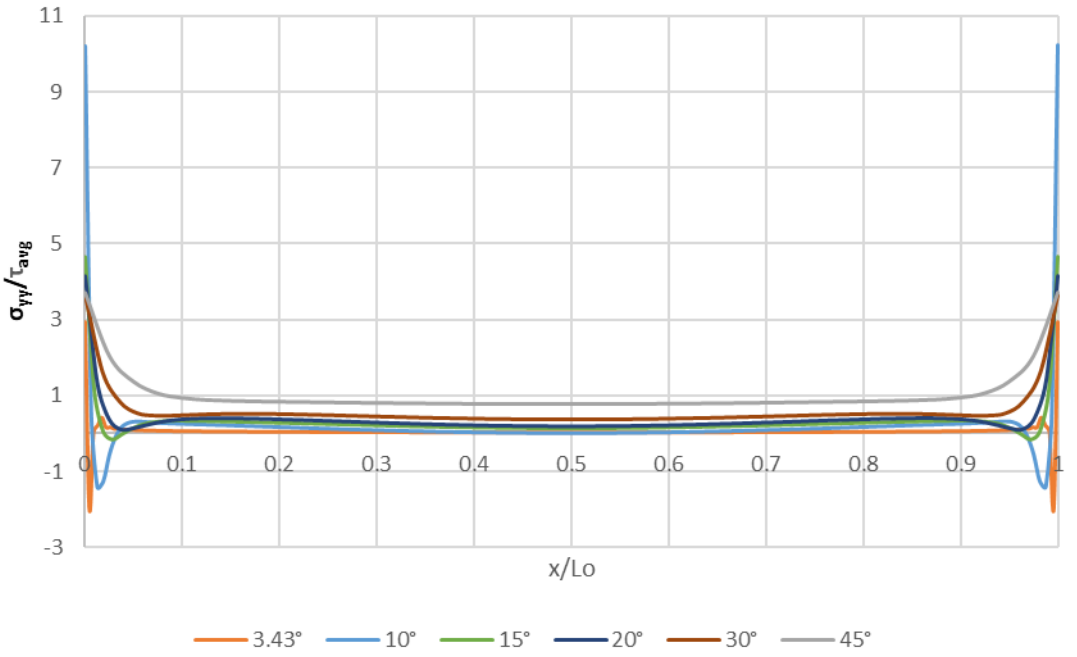

Figure 38 - Comparison of normalised peel stress in Araldite® AV138 across all angles at ΔT=80.

Stress distribution has the same pattern with the highest stress peaks in this adhesive. Therefore, the increase in temperature, increases stress at the adhesive free ends. On the other hand, as scarf angle increases, stress distribution improves. All the described behaviour is applicable for Araldite® 2015 and Sikaforce® 7752. As a result, the adhesives at ΔT=80 are compared, where peak stresses are the highest across.

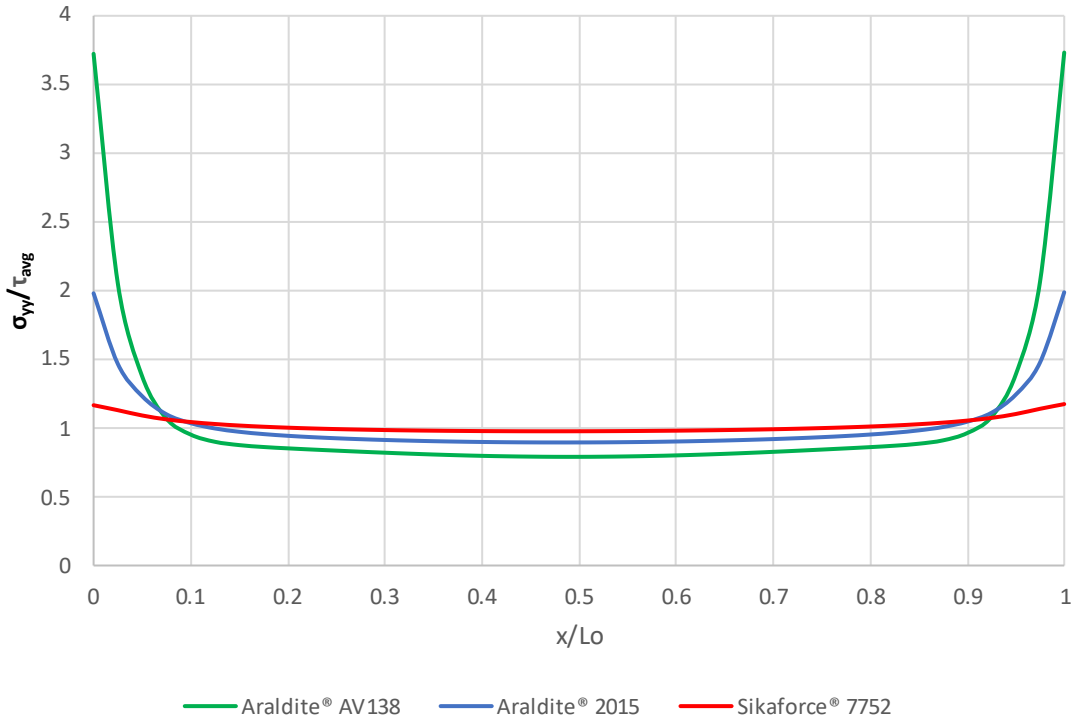

Figure 39 - Comparison of normalised peel stress in all adhesives at ΔT=80 and α=45°.

When comparing the adhesives (Figure 39), the peel stress peaks are the highest with Araldite® AV138 and Sikaforce® 7752, as the more ductile, has the more uniform stress distribution. Therefore, it is observed that this is directly related to the stiffness of the adhesive as it was in different joint configurations [100] and brittle adhesive with high fragility [101] as peak stresses are high at the adhesive free ends.

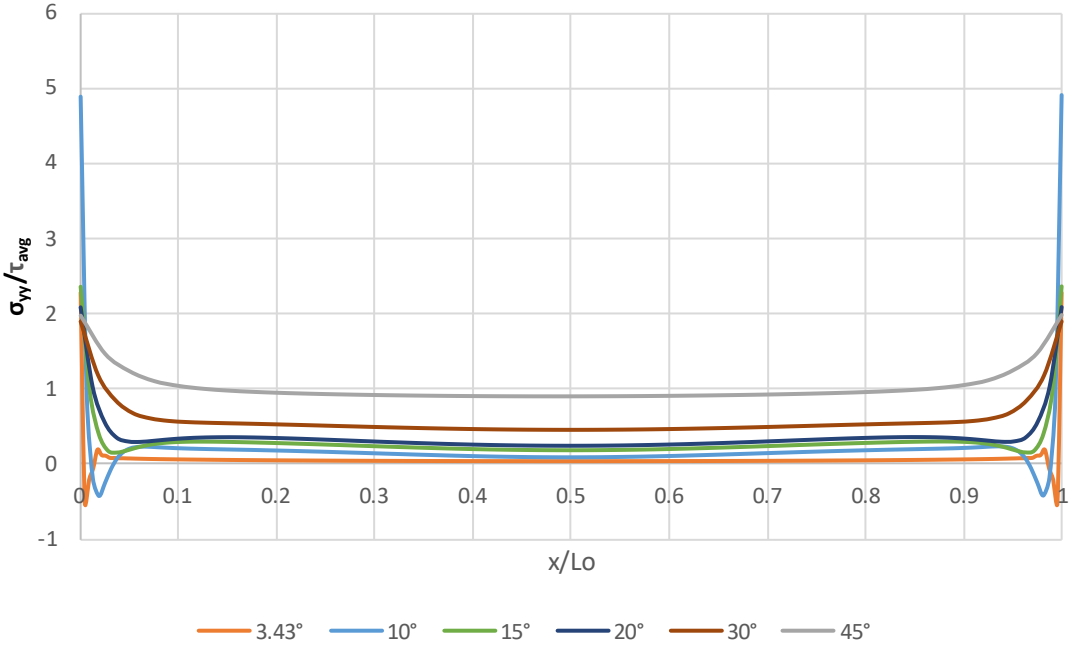

Figure 40 - Comparison of normalised peel stress in Araldite® 2015 across all angles at ΔT=80.

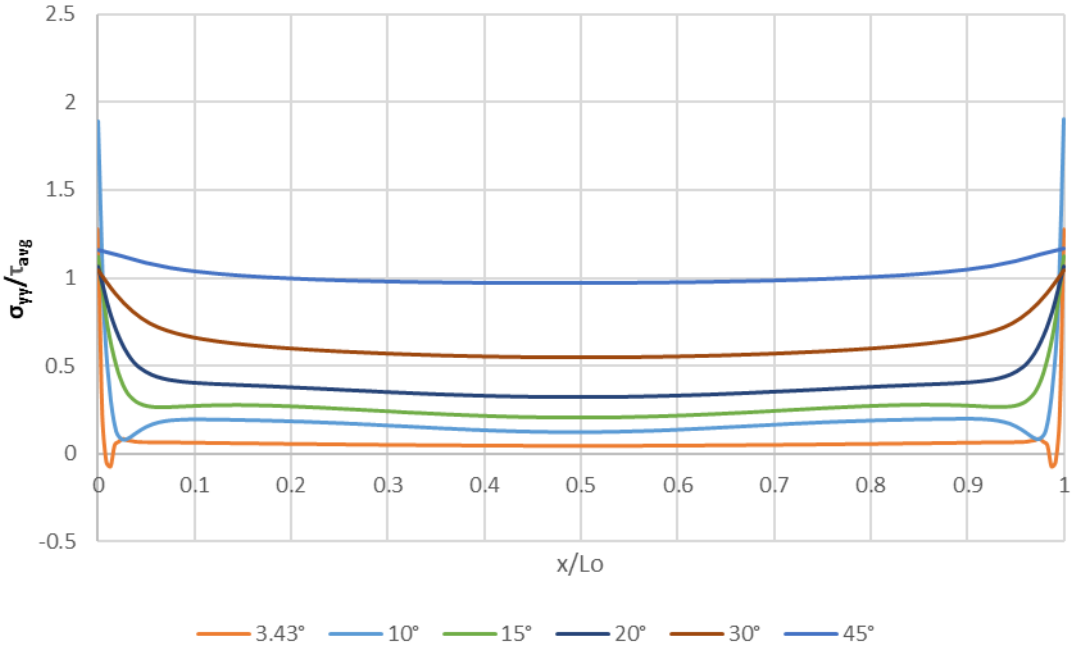

Figure 41 - Comparison of normalised peel stress in Sikaforce® 7752 across all angles at ΔT=80.

The behaviour, in Figure 40, Figure 41, is identical to what was described in the adhesive Araldite® AV138. So, it is observed that:

- stress distribution is a function of angle and temperature;
- peak stresses are a function of angle, temperature, and adhesive stiffness. These are localised at the free ends.

There's an improvement in stress distribution, however, its average also increases to value close to τ_{avg} as α=45° may provide identical stress preponderance [102] with an average increase of 1000%, from 3.43° to 45°, in the middle of the adhesive layer. At lower angles the orientation of stress is closer to shear stress in the adhesive layer.

The analysis of normalised shear stress starts with an analysis of the adhesives at α=3.43° and ΔT=0 (Figure 42). Although it has the higher peaks due to its stiffness, Araldite® AV138 has a much smoother transition into the middle layer compared to the others, however, it may not have enough ductile properties to sustain failure.

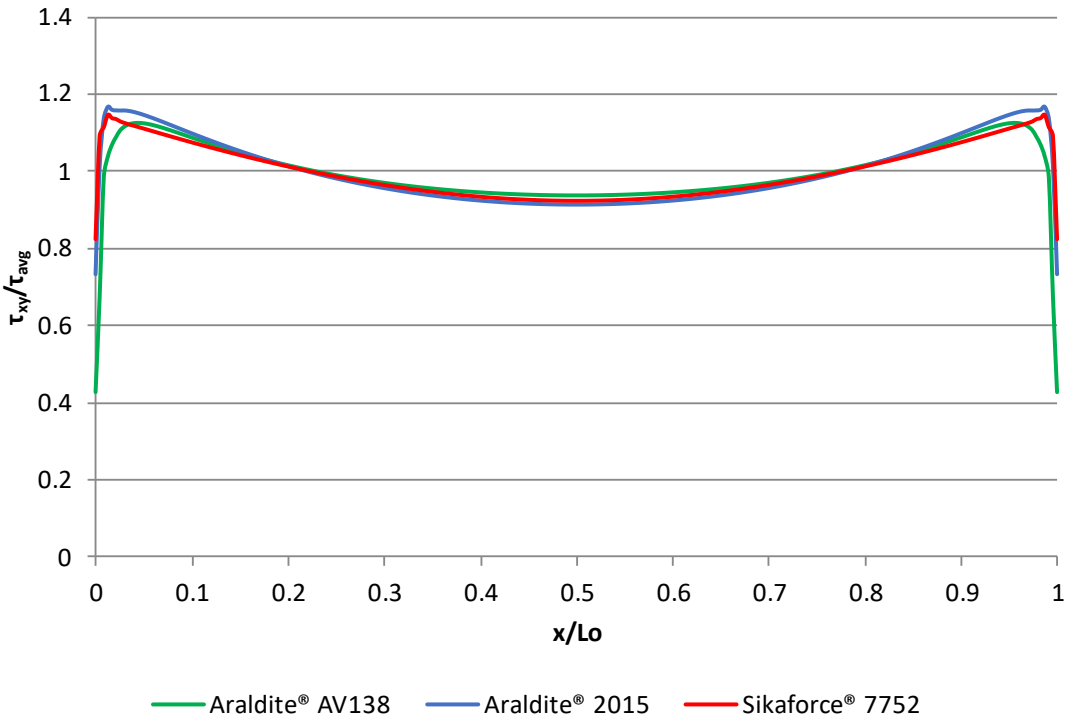

Figure 42 - Comparison of normalised shear stress at α=3.43° and ΔT=0, in function of stiffness (adhesive).

At RT, it appears that a function of α does not exist, nevertheless, stress distribution is more uniform as α increases (Figure 43). Nevertheless, as temperature rises (Figure 44 and Figure 45), peak stresses increase, however, stress distribution in the middle part improves.

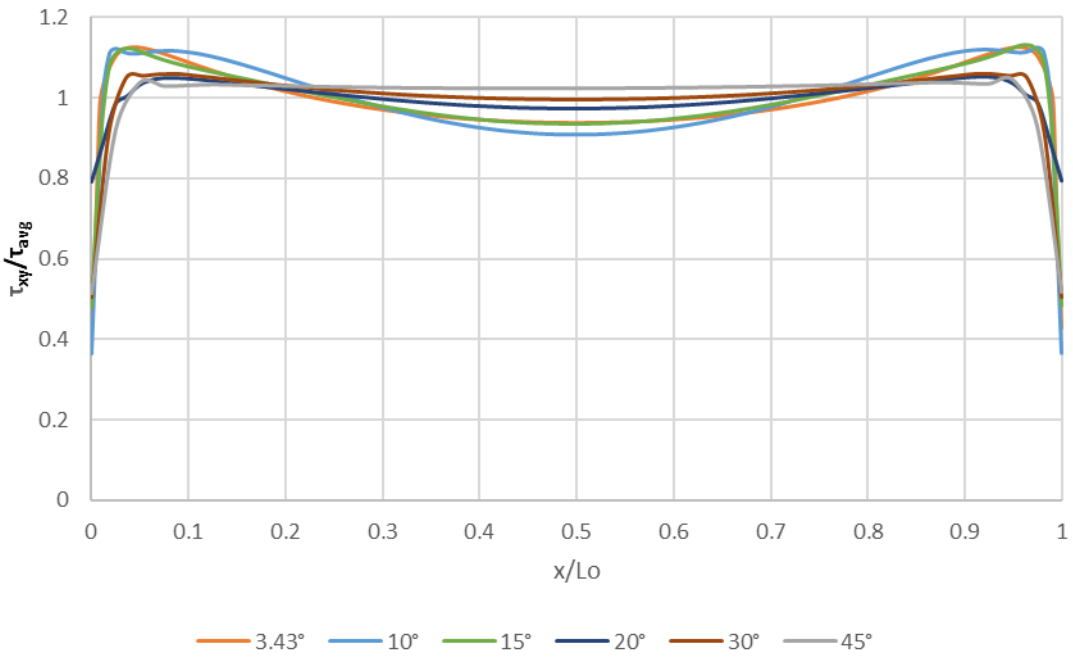

Figure 43 - Comparison of normalised shear stress in Araldite® AV138 across all angles at ΔT=0.

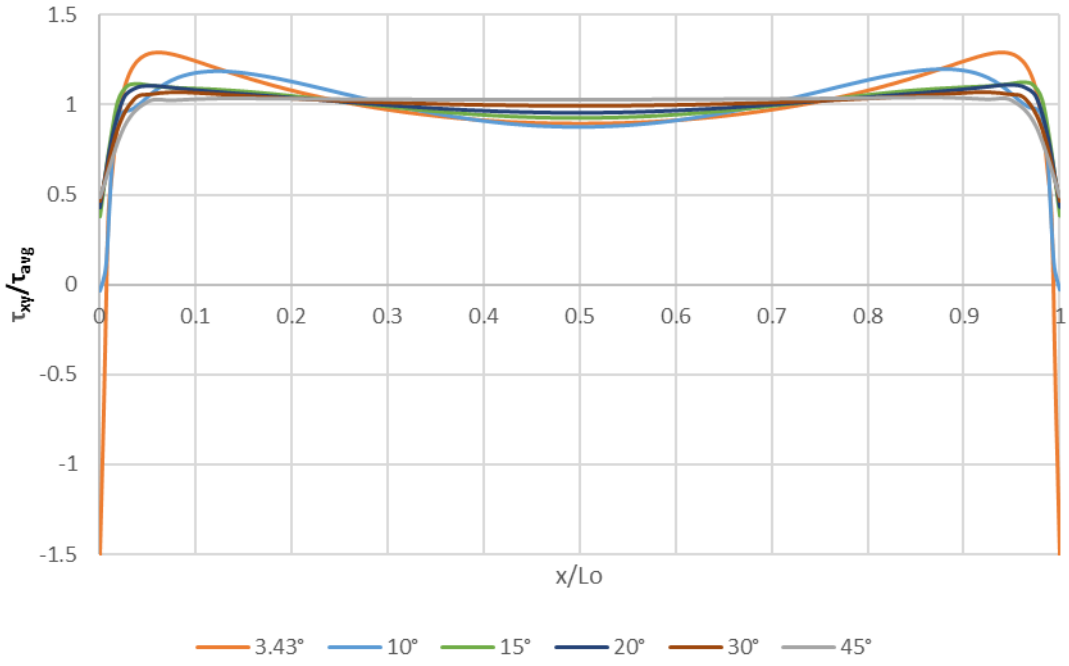

Figure 44 - Comparison of normalised shear stress in Araldite® AV138 across all angles at ΔT=40.

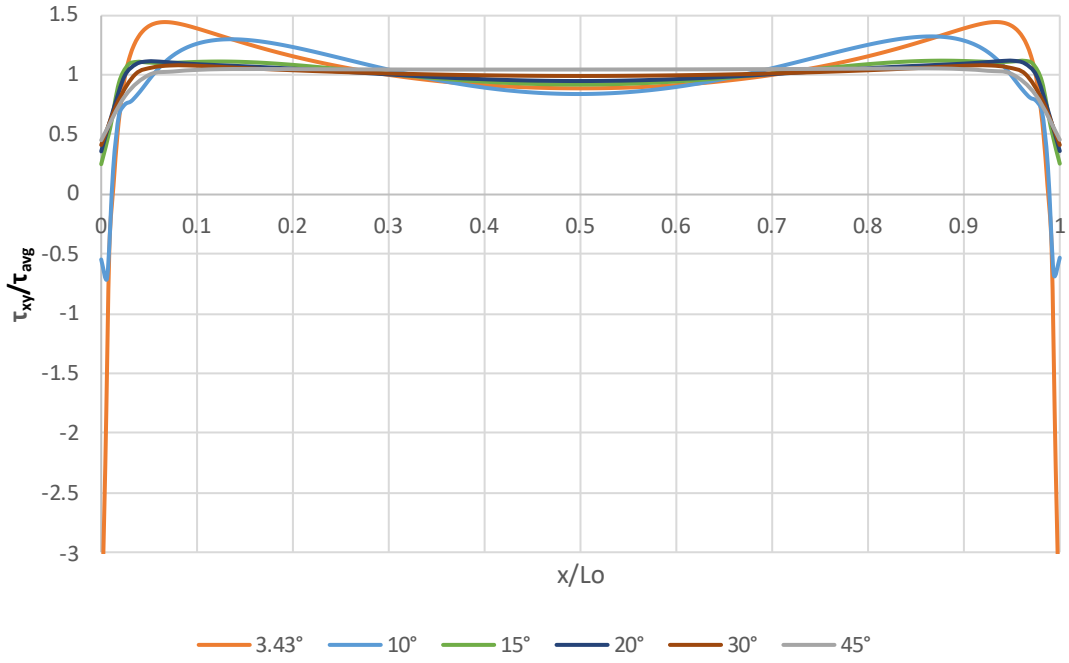

Figure 45 - Comparison of normalised shear stress in Araldite® AV138 across all angles at ΔT=80.

So, a comparison is made where both conditions that increase peak stress in function of the adhesive and, therefore, stiffness (Figure 46).

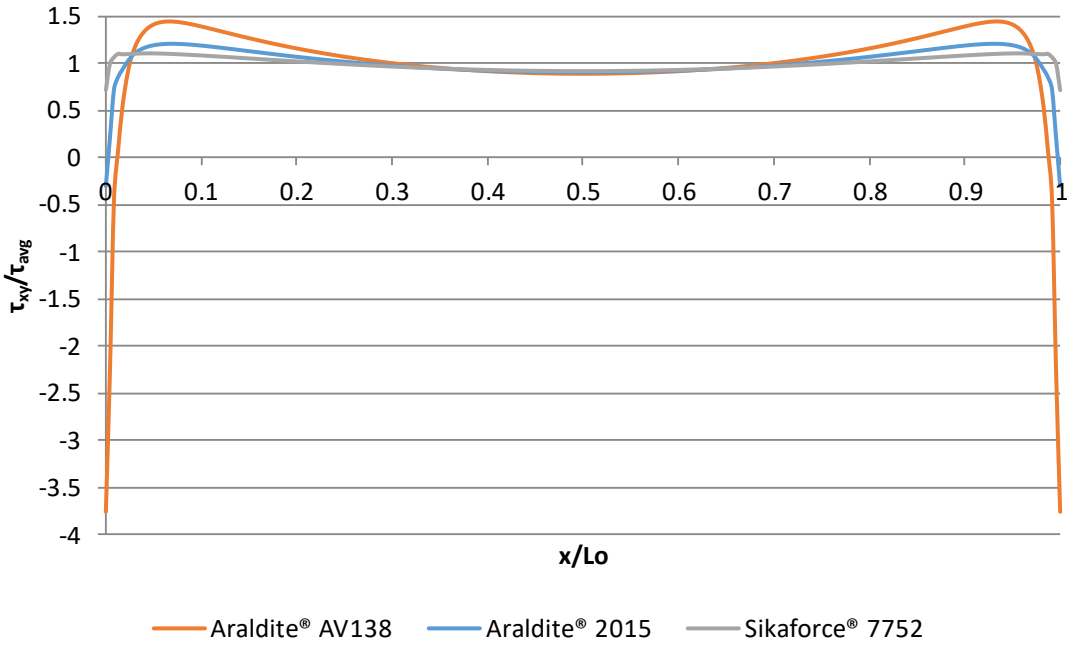

Figure 46 - Comparison of normalised shear stress at α=3.43° and ΔT=80, in function of stiffness (adhesive).

It is observed that stress distribution is more uniform with Sikaforce® 7752 and the highest peak stress are with Araldite® AV138, which means that higher stiffness has a greater influence on the differential deformation of the adherends at the adhesive free ends [102].

In conclusion, in both peel and shear stress,

- stress distributions are a function of α and stiffness, which means, that
  - the increase in angle improves stress distribution and
  - the increase in stiffness decreases stress distribution;
- peak stresses are at the adhesive free ends and, also, are a function of ΔT, α and stiffness, which means, that
  - the increase in temperature, increases peak stress,
  - the decrease in angle, increases peak stress, as well and
  - the increase in stiffness, increases peak stress, too.

However, lower scarf angle exponentially increases the length of the adhesive layer which can override the described effect due to a large increase in joint strength [103].

4.3. Damage variable study

In this subchapter, the SDEG damage variable study is presented to the different configurations. This study of the cohesive elements in the adhesive layer is another form of comparison of, in this case, the scarf joint configuration bonded with different stiffness adhesives at three moments of temperature. The variable ranges from 0 (undamaged) to 1 (complete failure) which helps to understand stiffness degradation of the cohesive law in mix mode of the CZM.

In Figure 47, Figure 48, SDEG is compared, at room temperature, between the adhesives Araldite® AV138, Araldite® 2015 and Sikaforce® 7752 at α=3.43°. It is observed that damage has the higher incidence at the adhesive free ends and the increase in stiffness, the magnitude of the damage increases and is concentrated in smaller areas at the ends of the bond, showing more oscillations. On the other hand, the increased ductility of the adhesive allows for a more uniform distribution of damage at the distribution at P_{max}, therefore, a better adhesive utilisation over the bond length.

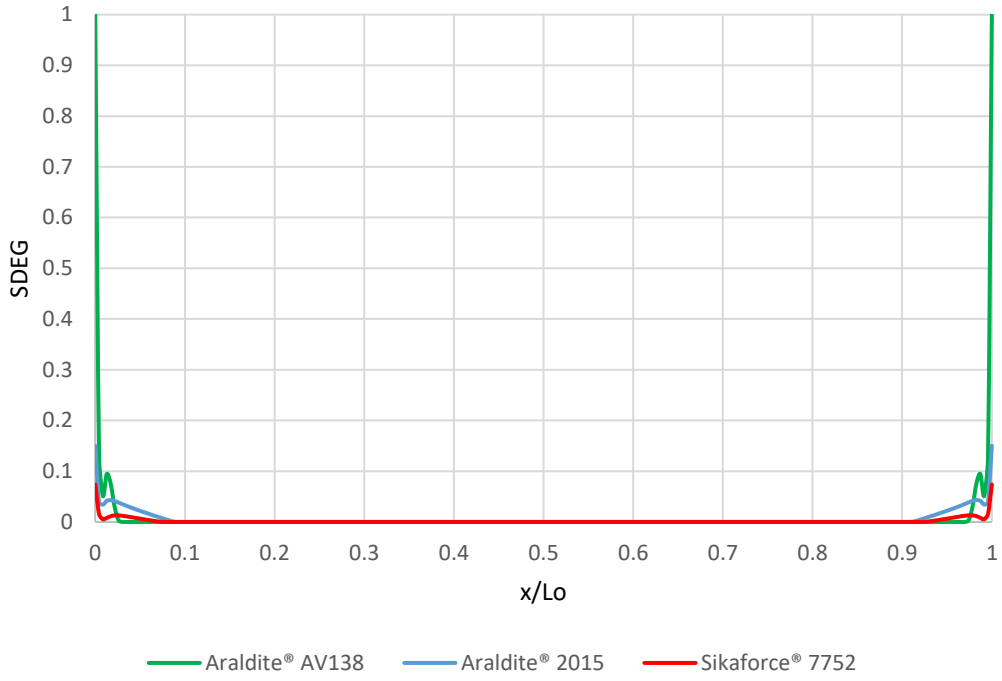

Figure 47 - Comparison of the SDEG variable at ΔT=0 and α=3.43°, in function of the adhesive.

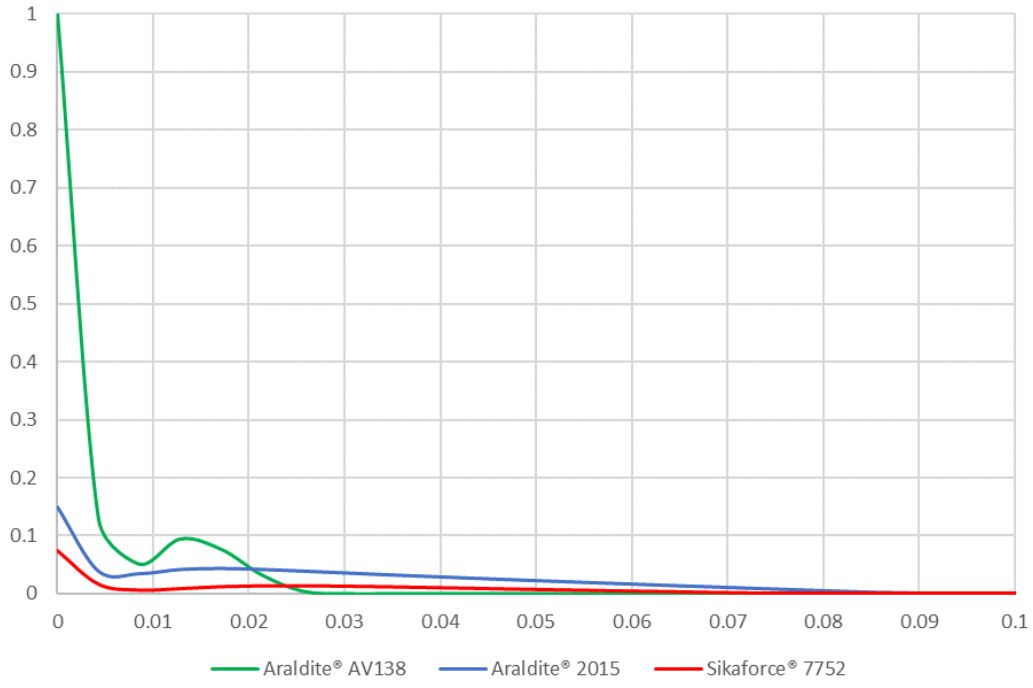

Figure 48 – Zoomed portion of Figure 47 (adhesive free end).

In Figure 49, Figure 50 and Figure 51, Figure 52, SDEG is compared in the adhesives Araldite® AV138 and Sikaforce® 7752, respectively, at α=3.43°, in function of ΔT. It is observed that as ΔT increases, the localised magnitude of damage at the free ends increases and it is increasingly less uniform along the adhesive layer.

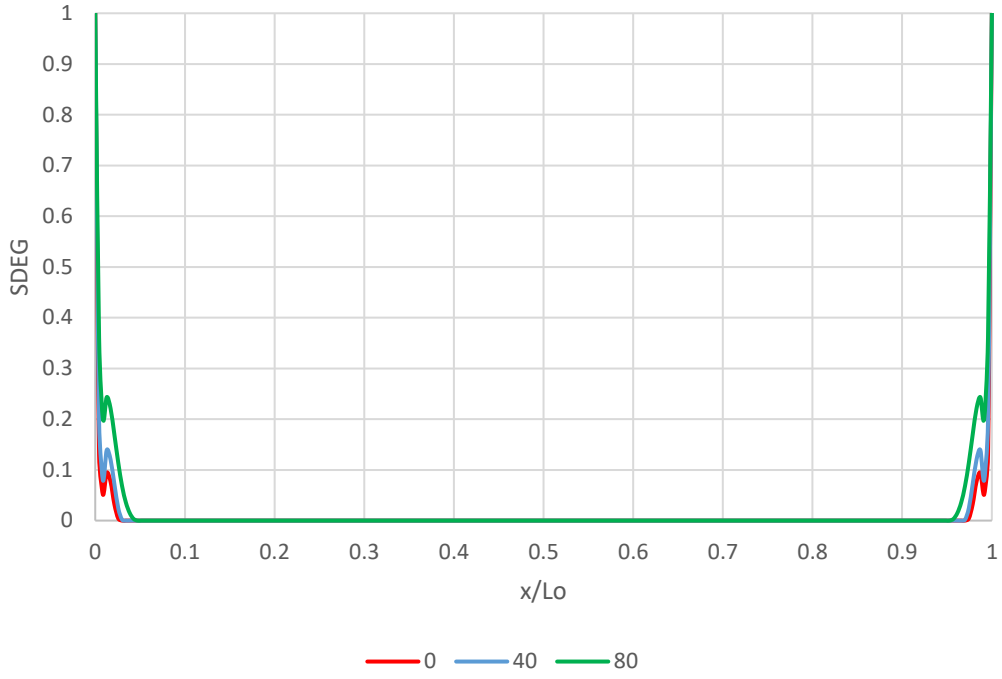

Figure 49 - Comparison of the SDEG variable in Araldite® AV138 at α=3.43°, in function of ΔT.

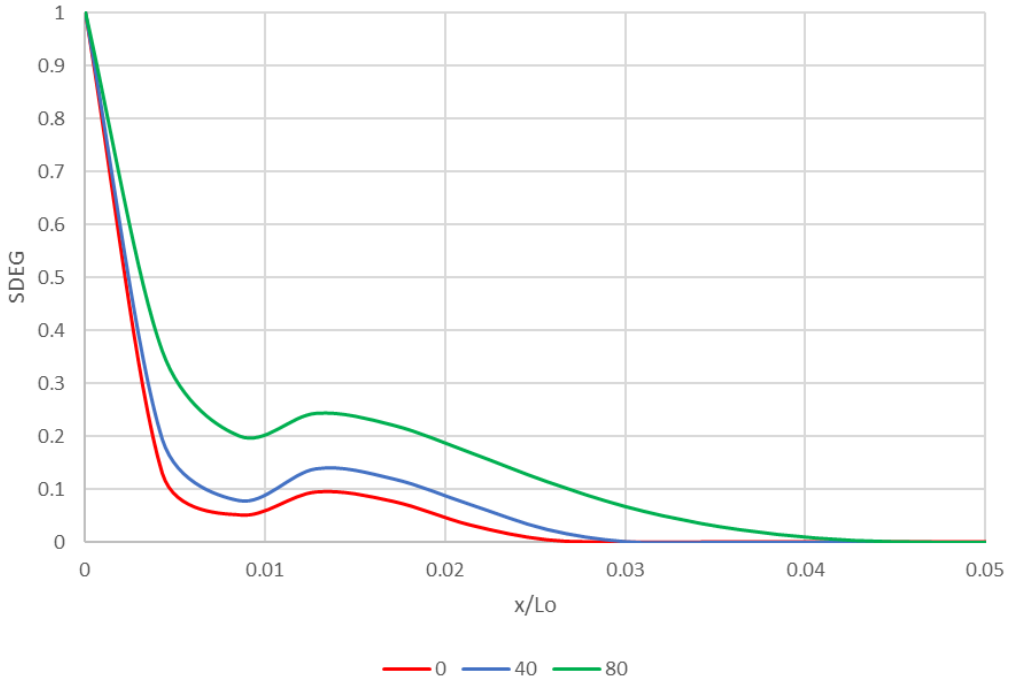

Figure 50 - Zoomed portion of Figure 49 (adhesive free end).

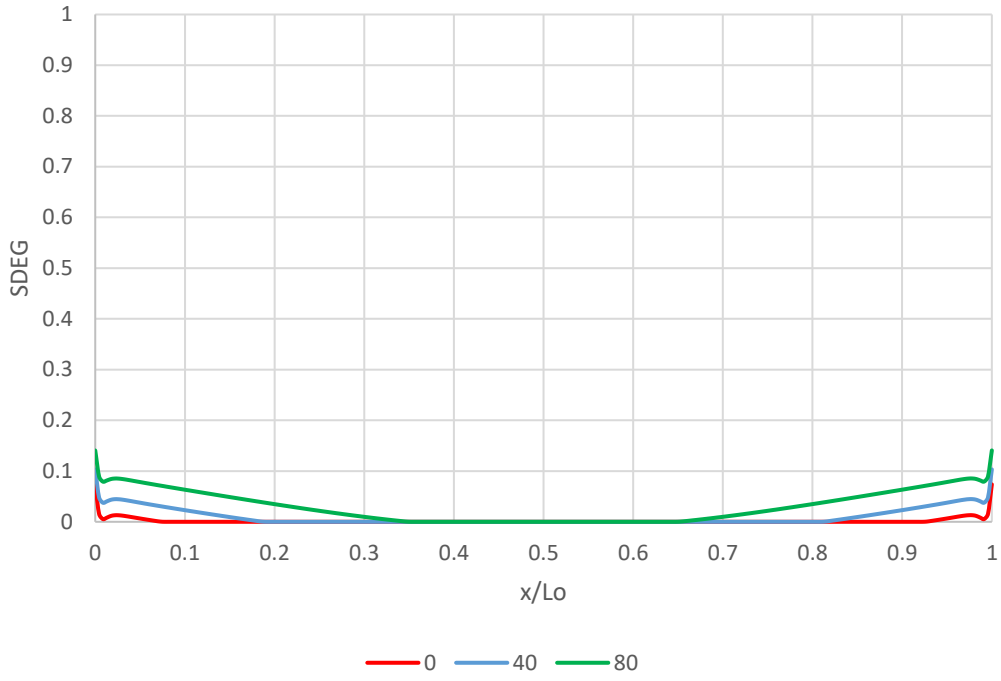

Figure 51 - Comparison of the SDEG variable in Sikaforce® 7752 at α=3.43°, in function of ΔT.

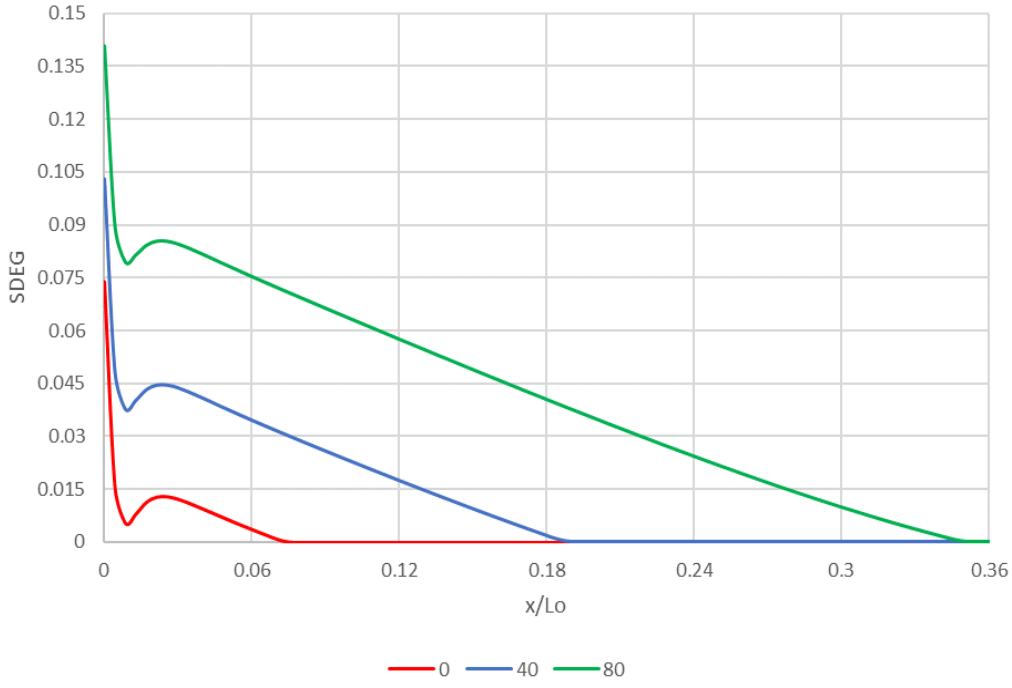

Figure 52 - Zoomed portion of Figure 51 (adhesive free end).

In Figure 53, Figure 54, SDEG is compared in the adhesive Araldite® 2015 at ΔT=80, in function of α. It is observed that as α increases, the localised magnitude of damage at the free ends decreases and it is increasingly more uniform along the adhesive layer.

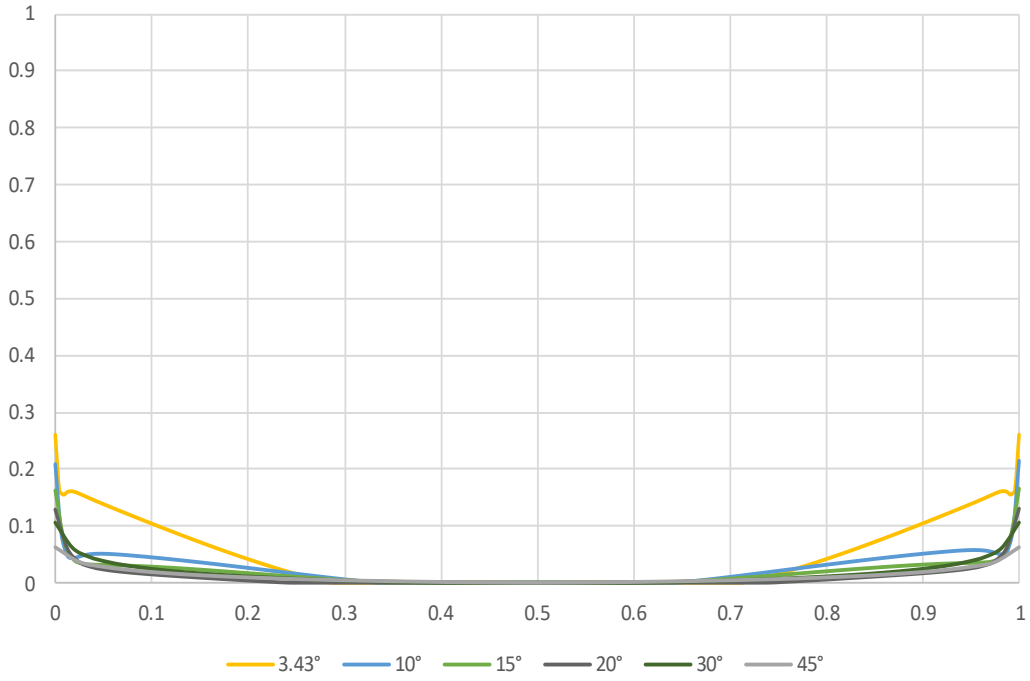

Figure 53 - Comparison of the SDEG variable in Araldite® 2015 at ΔT=80, in function of α.

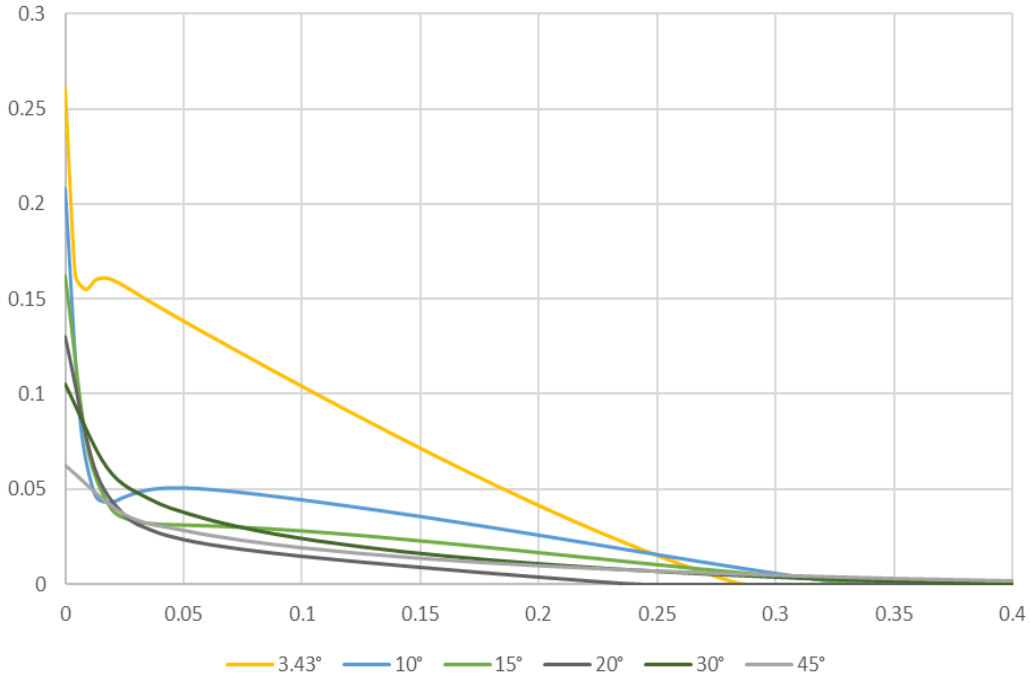

Figure 54 - Zoomed portion of Figure 53 (adhesive free end).

In conclusion,

- the increase in temperature, increases localised magnitude of damage and damage distribution is increasingly worse,
- the increase in angle, decreases localised magnitude of damage and damage distribution is increasingly better and

- the increase in stiffness, increases localised magnitude of damage and damage distribution is increasingly worse.

So, the variable SDEG is a function of ΔT, α and stiffness, with similar effects in the localised magnitude of damage at the free ends and damage distribution along the adhesive layer.

4.4. Failure modes

In this subchapter, failure modes are presented and analysed. There were obtained in ABAQUS® software. In the literature, experimental testing has shown that it is adhesive failure [104, 105]. In Figure 55, Figure 56 and Figure 57, failure mode in SJs bonded with Araldite® AV138 at 3.43° is presented, in function of ΔT. As previous analysed, this is combination has highest strength. It is observed that SDEG maxes out at 1, which means that failure is achieved, and it is cohesive. Cohesive failure means that the strength of the bond between the adherend and the adhesive is greater than the internal strength of the adhesive.

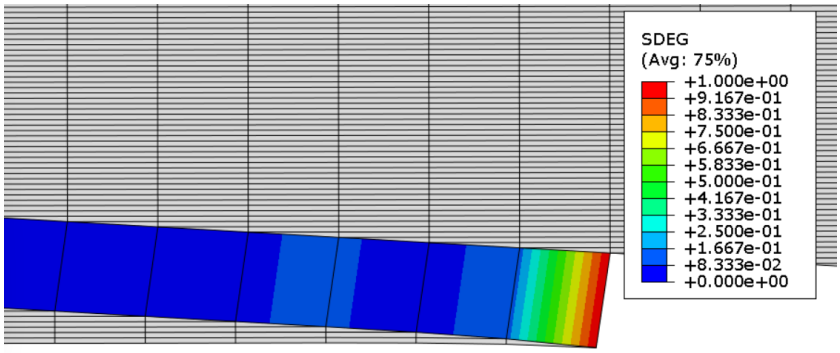

Figure 55 - Failure mode in SJ bonded with Araldite® AV138 at α=3.43 and ΔT=0.

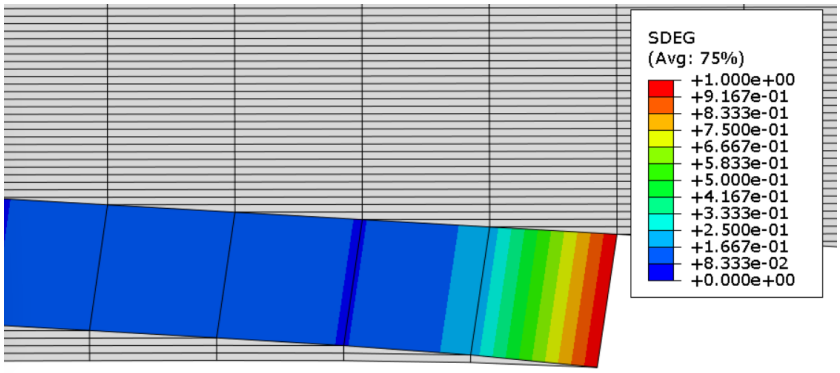

Figure 56 - Failure mode in SJ bonded with Araldite® AV138 at α=3.43 and ΔT=40.

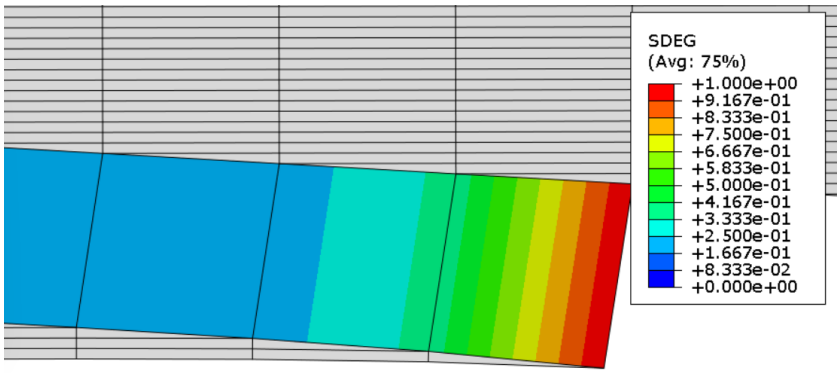

Figure 57 - Failure mode in SJ bonded with Araldite® AV138 at α=3.43 and ΔT=80.

4.5. Strength prediction

In this section, an analysis is presented to evaluate the CZM ability in predicting the strength of the scarf adhesive joints in study here. Therefore, the P-δ curves are presented to understand how temperature and scarf angle may influence the strength of the joint and compare performance between adhesives, as well. P-δ curves are obtained by combining all the reaction forces, due to pulling, that occurred in the numerical analysis with the resulting displacement. In general, force is in the y-axis (ordinate) while displacement is represented in the x-axis (abscissa). In Figure 58, P_{max} values are presented for all adhesives, Araldite® AV138, Araldite® 2015 and Sikaforce® 7752 at RT, in function of α. It is observed that P_{max} is higher at 3.43° and decreases as the angle increases, for all adhesives. These are the highest with Araldite® AV138.

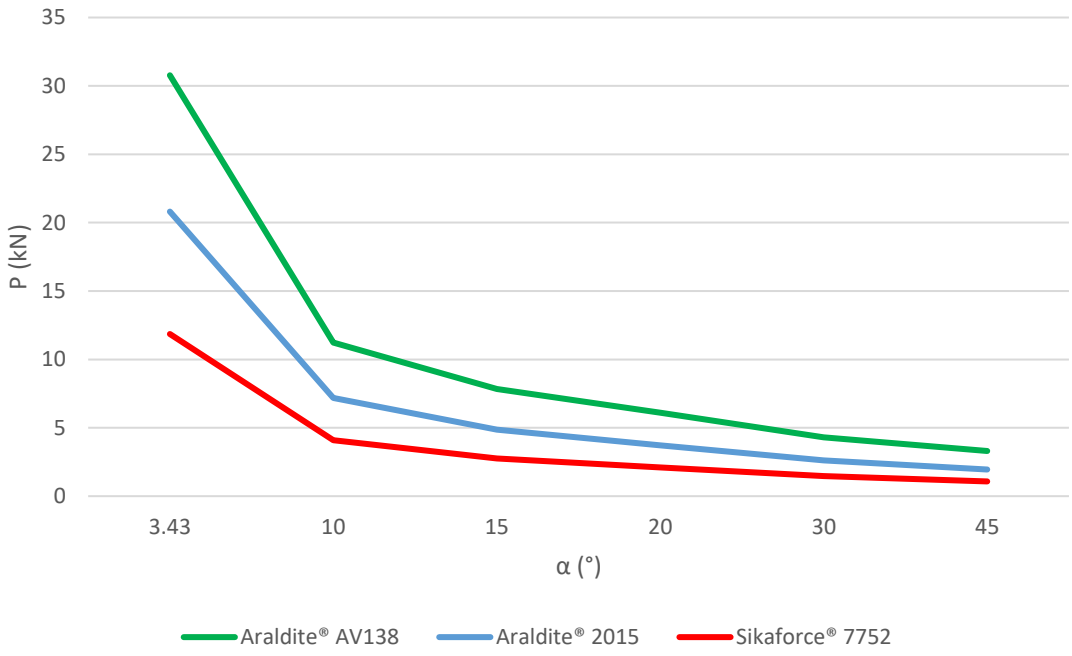

Figure 58 - Pmax values distribution for all adhesives at ΔT=0, in function of α.

In Figure 59, the variable temperature is introduced at the combination of adhesive and angle with higher P_{max} values (Figure 58). It is observed that P_{max} values have a slight variation due to the temperature increase; however, it could be considered negligible. This behaviour repeats

across all angles. Nevertheless, temperature increases displacement at failure due to dilatation of the adhesive layer, reflected in the overall displacement, with a mean magnitude of 0.234 mm.

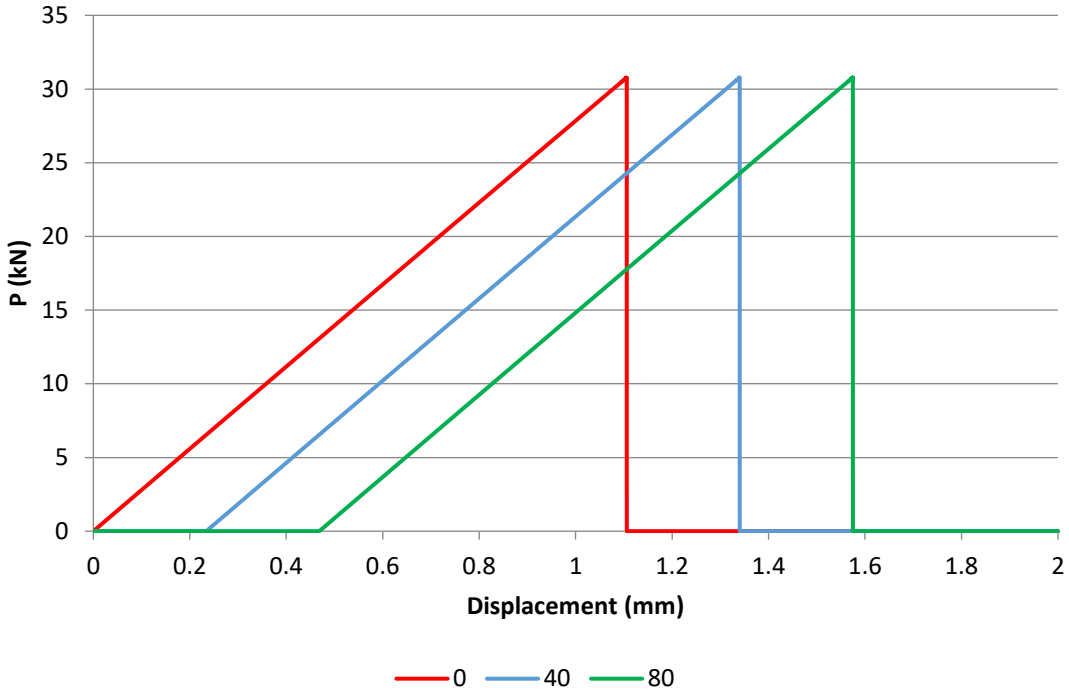

Figure 59 - Comparison of P-δ curves of Araldite® AV138 at 3.43°, in function of ΔT.

In Figure 60, the variable temperature is removed and at RT, in function of α, it was observed that, like in Figure 58, the more brittle adhesive, Araldite® AV138, has the highest P_{max} and displacement at failure.

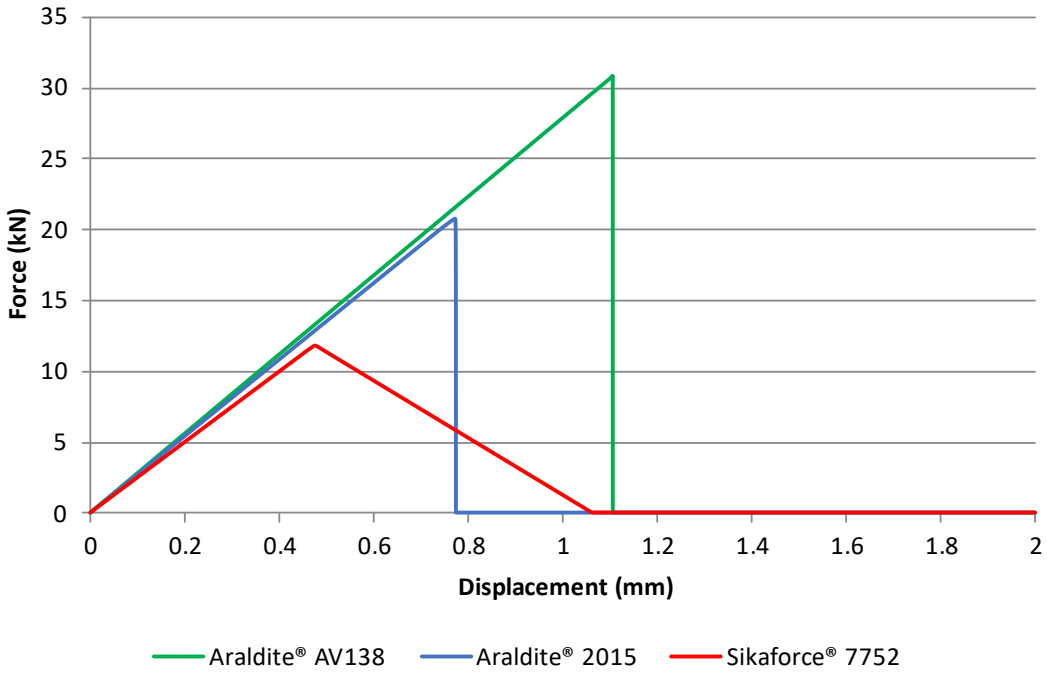

Figure 60 - Comparison of P-δ curves at ΔT=0 and 3.43°, in function of the adhesive.

In Figure 61, P-δ curves are compared, at ΔT=80, in Araldite® 2015 and in Figure 62, at ΔT=0, in Sikaforce® 7752, both in function of α. As pointed before, Pmax increases with the decrease in angle. Also, it is observed an evolution in the P-δ curves after failure which is more pronounced Sikaforce® 7752. It happens due to a uniform adhesive stress, resulting in the transposition of the cohesive law to P-d curves.

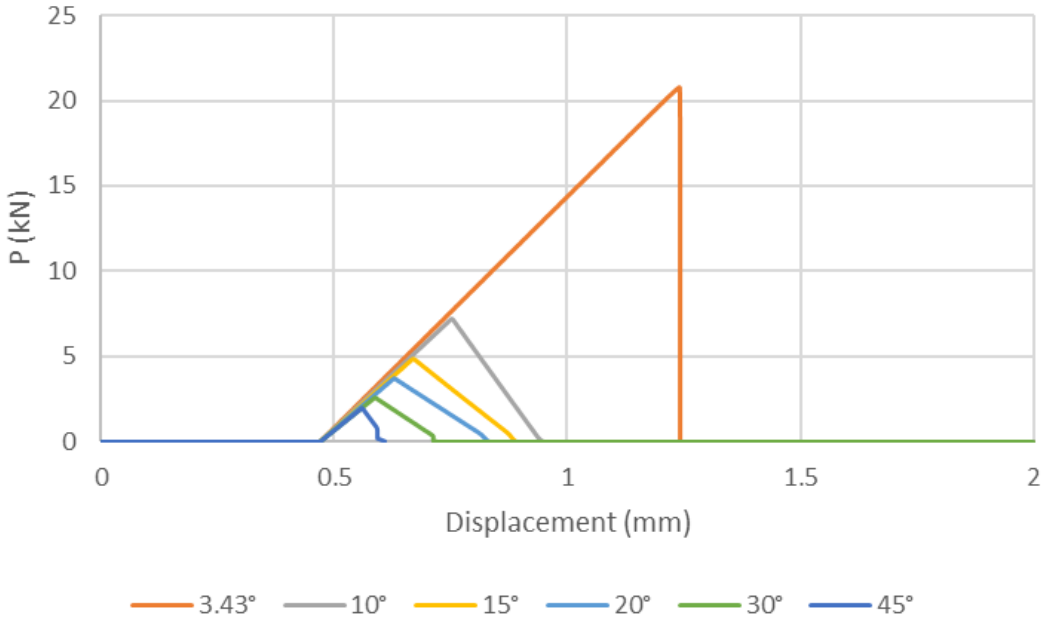

Figure 61 - Comparison of P-d curves of Araldite® 2015 at ΔT=80, in function of α.

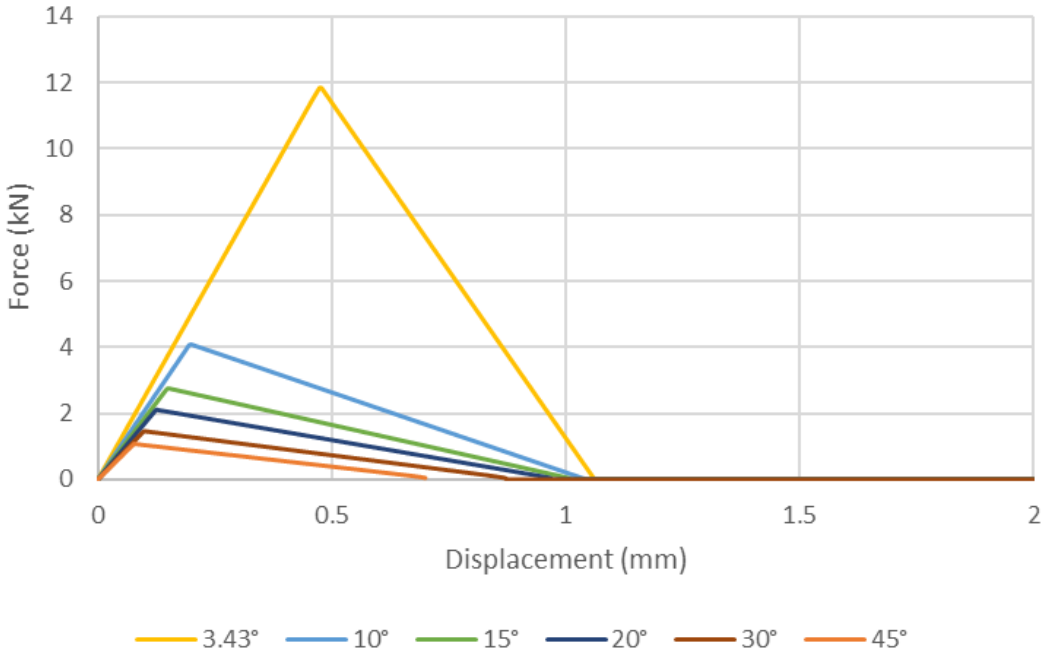

Figure 62 - Comparison of P-δ curves of Sikaforce® 7752 at ΔT=0, in function of α.

In conclusion, strength is a function of α and stiffness, which means, that

- the increase in α,

  - reduces strength and
  - reduces displacement at failure, due to a decrease in the bonded area;
- the increase in stiffness,
  - led to higher P_{max} values, therefore, Araldite® AV138 had the highest and
  - increases displacement at failure.

Although, temperature does not have an effect in strength, it has in displacement at failure, with mean increases, per 40 points, of 0.234 mm, due to adhesive expansion.

4.6. Joints' dissipated energy

François Roddier said that "*the conversion of mechanical energy into heat is called energy dissipation".* That energy is defined as the area below the *P-*δ curves and it is calculated using the trapezoidal rule.

Based on the data presented in 3.2.1, it is assumed that dissipated energy values are not influenced by ΔT, the smaller α have more dissipated energy and AV138 has more than 2015, which in turn will be higher than 7752. However, E_{diss} is based on stiffness and scarf angle (Figure 63). At 3.43°, it is identical to what was observed in the analysis of P_{max} but it is noticeable a smaller difference between Araldite® 2015 and Sikaforce® 7752. This difference becomes more evident as the scarf angle increases, where at α=10°, the adhesive Sikaforce® 7752 has more dissipated energy than Araldite® 2015, and at α=15°, it has more than Araldite® AV138.

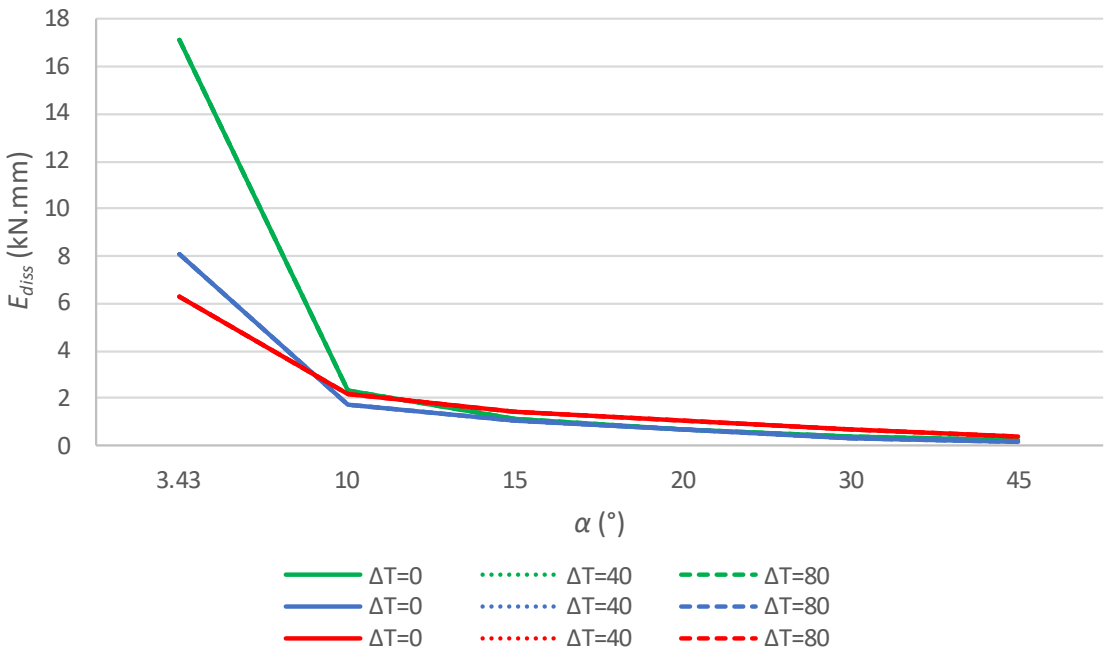

Figure 63 - Comparison of energy dissipated across all angles, ΔT and adhesives (Araldite® AV138, in green; Araldite® 2015, in blue; Sikaforce® 7752, in red).

In conclusion,

- as scarf angles decreases (therefore, bonded area increases), energy dissipation increases;
- the highest value is observed in the more brittle adhesive (Araldite® AV138) at 3.43°;
- the more ductile adhesive (Sikaforce® 7752) had the higher energy dissipation values from angles of 15° and higher;
- temperature does not have an effect in energy dissipation.

5. CONCLUSIONS AND FUTURE WORK PROPOSALS

5.1. Conclusions

The main goal of this study is to understand the how temperature affects strength in scarf adhesive joints, in which three adhesives of different strength and stiffness were considered through different values of α. The three adhesives used were Araldite® AV138, a brittle epoxy, Araldite® 2015, a ductile epoxy, and Sikaforce®7752, a polyurethane ductile epoxy, and Sikaforce®7752, a polyurethane that combines high ductility and moderate strength. The numerical study focused on the analysis of stress distributions, σ_{yy} and τ_{xy}, SDEG, strength and dissipated energy.

Firstly, the choice of adhesive is the most important factor and Araldite® AV138 was the one where the highest P_{max} was observed. This correlates with the fact that SJ geometry takes advantage of this high strength adhesive. However, this brittle adhesive has higher peak stress and localised magnitude of damage with stress and damage distribution less uniform due to its stiffness.

Scarf angle has significant implications, as well, where at lower values the peak stresses at the adhesive free ends are higher and stress distribution is not as uniform. The same effect is present in SDEG with the localised magnitude of damage at the free ends and damage distribution along the adhesive layer. Nevertheless, P_{max} is the highest due to a higher area adhesive layer and it translates into more energy dissipation.

Temperature has no significant effect in P_{max}, however, it increases peak stresses and localised magnitude of damage at the adhesive free ends, but it has in displacement at failure which increased 0.234 mm, in average.

It can be concluded that CZM is a precise technique in predicting strength of different joint geometries for the various adhesives, because it allows detailed analysis of stresses and damage.

5.2. Future work proposals

In future works, it is presented the following suggestions:

- The numerical study of different configurations of substrates and adhesives;
- The numerical study at different loads and temperatures;
- The variation in the geometric parameterisation.

REFERENCES

1. Van Rijn, L.P.V.M., *6.13 - Design of Sailplanes Using Composite Materials*, in *Comprehensive Composite Materials*, A. Kelly and C. Zweben, Editors. 2000, Pergamon: Oxford. p. 243-277.
2. Duncan, B., *14 - Developments in testing adhesive joints*, in *Advances in Structural Adhesive Bonding*, D.A. Dillard, Editor. 2010, Woodhead Publishing. p. 389-436.
3. Kwon, Y.W., *8.9 Design and Analysis of Bonded Joints and Repair*, in *Comprehensive Composite Materials II*, P.W.R. Beaumont and C.H. Zweben, Editors. 2018, Elsevier: Oxford. p. 157-177.
4. Kwon, Y.W., *24 - Computational and experimental study of composite scarf bonded joints*, in *Structural Integrity and Durability of Advanced Composites*, P.W.R. Beaumont, C. Soutis, and A. Hodzic, Editors. 2015, Woodhead Publishing. p. 659-693.
5. Liao, L., C. Huang, and T. Sawa, *Effect of adhesive thickness, adhesive type and scarf angle on the mechanical properties of scarf adhesive joints.* International Journal of Solids and Structures, 2013. **50**(25): p. 4333-4340.
6. Silva, D.F.O., R.D.S.G. Campilho, F.J.G. Silva, and U.T.F. Carvalho, *Experimental and numerical analysis of scarf aluminum adhesive joints.* Procedia Manufacturing, 2018. **17**: p. 705-712.
7. Goh, J.Y., S. Georgiadis, A.C. Orifici, and C.H. Wang, *Effects of bondline flaws on the damage tolerance of composite scarf joints.* Composites Part A: Applied Science and Manufacturing, 2013. **55**: p. 110-119.
8. Bendemra, H., P. Compston, and P.J. Crothers, *Optimisation study of tapered scarf and stepped-lap joints in composite repair patches.* Composite Structures, 2015. **130**: p. 1-8.
9. Apalak, M.K. and R. Gunes, *On non-linear thermal stresses in an adhesively bonded single lap joint.* Computers & Structures, 2002. **80**(1): p. 85-98.
10. Zhao, N., L. Cao, H. Guo, Q. Jia, and J. Dai, *Numerical Analysis on the Temperature and Thermal Stress Distribution in Adhesive Joints*. 2008. p. 71-80.
11. Na, J., W. Mu, G. Qin, W. Tan, and L. Pu, *Effect of temperature on the mechanical properties of adhesively bonded basalt FRP-aluminum alloy joints in the automotive industry.* International Journal of Adhesion and Adhesives, 2018. **85**: p. 138-148.
12. Machado, J.J.M., P.D.P. Nunes, E.A.S. Marques, and L.F.M. da Silva, *Adhesive joints using aluminium and CFRP substrates tested at low and high temperatures under quasi-static and impact conditions for the automotive industry.* Composites Part B: Engineering, 2019. **158**: p. 102-116.
13. Agarwal, A., S.J. Foster, and E. Hamed, *Wet thermo-mechanical behavior of steel–CFRP joints – An experimental study.* Composites Part B: Engineering, 2015. **83**: p. 284-296.
14. Agarwal, A., S.J. Foster, and E. Hamed, *Testing of new adhesive and CFRP laminate for steel-CFRP joints under sustained loading and temperature cycles.* Composites Part B: Engineering, 2016. **99**: p. 235-247.
15. Qin, G., J. Na, W. Mu, W. Tan, J. Yang, and J. Ren, *Effect of continuous high temperature exposure on the adhesive strength of epoxy adhesive, CFRP and adhesively bonded CFRP-aluminum alloy joints.* Composites Part B: Engineering, 2018. **154**: p. 43-55.
16. Volkersen, O., *Die Niektraftverteilung in zugbeanspruchten mit konstanten laschenquerschritten.* Luftfahrtforschung, 1938. **15**: p. 41-47.
17. da Silva, L.F.M., P.J.C. das Neves, R.D. Adams, and J.K. Spelt, *Analytical models of adhesively bonded joints—Part I: Literature survey.* International Journal of Adhesion and Adhesives, 2009. **29**(3): p. 319-330.
18. da Silva, L.F.M., A.G. de Magalhães, and M.F.S.F. de Moura, *Juntas Adesivas Estruturais*. 2007, Porto: Publindústria.
19. Goland, M. and E. Reissner, *The stresses in cemented joints.* Journal of Applied Mechanics, 1944(66): p. A17-A27.

20. Hart-Smith, L.J., *Adhesive-Bonded Single-Lap Joints*. 1973, NASA CR-112236.
21. da Silva, J.F.M.G., A. Öchsner, and R.D. Adams, *Handbook of Adhesion Technology*. 2011, Heidelberg: Springer.
22. Renton, W.J. and J.R. Vinson, *Analysis of Adhesively Bonded Joints Between Panels of Composite Materials.* Journal of Applied Mechanics, 1977. **44**(1): p. 101-106.
23. Ojalvo, I.U. and H.L. Eidinoff, *Bond Thickness Effects upon Stresses in Single-Lap Adhesive Joints.* AIAA Journal, 1978. **16**(3): p. 204-211.
24. ALLMAN, D.J., *A THEORY FOR ELASTIC STRESSES IN ADHESIVE BONDED LAP JOINTS.* The Quarterly Journal of Mechanics and Applied Mathematics, 1977. **30**(4): p. 415-436.
25. Chen, D. and S. Cheng, *An Analysis of Adhesive-Bonded Single-Lap Joints.* Journal of Applied Mechanics, 1983. **50**(1): p. 109-115.
26. Adams, R.D. and V. Mallick, *A Method for the Stress Analysis of Lap Joints.* The Journal of Adhesion, 1992. **38**(3-4): p. 199-217.
27. Zhao, B. and Z.-H. Lu, *A Two-Dimensional Approach of Single-Lap Adhesive Bonded Joints.* Mechanics of Advanced Materials and Structures, 2009. **16**(2): p. 130-159.
28. Yang, C. and S.S. Pang, *Stress-Strain Analysis of Single-Lap Composite Joints Under Tension.* Journal of Engineering Materials and Technology, 1996. **118**(2): p. 247-255.
29. Crocombe, A.D., *Stress analysis for adhesive structures*, in *2nd World Congress on Adhesion and Related Phenomena*. 2002, The Adhesion Society: Florida. p. 17 - 19.
30. Adams, R.D., *Adhesive Bonding, Science, technology and applications*. 2005, Cambridge England: Woodhead Publishing.
31. da Silva, L.F.M. and R.D.S.G. Campilho, *Advances in Numerical Modelling of Adhesive Joints*, in *Advances in Numerical Modeling of Adhesive Joints*. 2012, Springer Berlin Heidelberg. p. 1-93.
32. Adams, R.D., J. Comyn, and W.C. Wake, *Structural adhesive joints in engineering*. 2nd ed. 1997, London: Chapman & Hall.
33. Zhao, X., R.D. Adams, and L.F.M. da Silva, *Single Lap Joints with Rounded Adherend Corners: Stress and Strain Analysis.* Journal of Adhesion Science and Technology, 2011. **25**(8): p. 819-836.
34. Zhao, X., R.D. Adams, and L.F.M. da Silva, *Single Lap Joints with Rounded Adherend Corners: Experimental Results and Strength Prediction.* Journal of Adhesion Science and Technology, 2011. **25**(8): p. 837-856.
35. da Silva, L.F.M., R.J.C. Carbas, G.W. Critchlow, M.A.V. Figueiredo, and K. Brown, *Effect of material, geometry, surface treatment and environment on the shear strength of single lap joints.* International Journal of Adhesion and Adhesives, 2009. **29**(6): p. 621-632.
36. Williams, M.L., *The stresses around a fault or crack in dissimilar media.* Bulletin of the Seismological Society of America, 1959. **49**(2): p. 199-204.
37. Fernlund, G. and J.K. Spelt, *Failure load prediction of structural adhesive joints.* International Journal of Adhesion and Adhesives, 1991. **11**(4): p. 213-227.
38. Shahin, K. and F. Taheri, *The strain energy release rates in adhesively bonded balanced and unbalanced specimens and lap joints.* International Journal of Solids and Structures, 2008. **45**(25–26): p. 6284-6300.
39. Dillard, D.A., H.K. Singh, D.J. Pohlit, and J.M. Starbuck, *Observations of Decreased Fracture Toughness for Mixed Mode Fracture Testing of Adhesively Bonded Joints.* Journal of Adhesion Science and Technology, 2009. **23**(10-11): p. 1515-1530.
40. Rice, J.R. and G.F. Rosengren, *Plane strain deformation near a crack tip in a power-law hardening material.* Journal of the Mechanics and Physics of Solids, 1968. **16**(1): p. 1-12.
41. Barenblatt, G.I., *The formation of equilibrium cracks during brittle fracture. General ideas and hypotheses. Axially-symmetric cracks.* Journal of Applied Mathematics and Mechanics, 1959. **23**(3): p. 622-636.

42. Barenblatt, G.I., *The Mathematical Theory of Equilibrium Cracks in Brittle Fracture*, in *Advances in Applied Mechanics*, T.v.K.G.K.F.H.v.d.D. H.L. Dryden and L. Howarth, Editors. 1962, Elsevier. p. 55-129.
43. Dugdale, D.S., *Yielding of steel sheets containing slits.* Journal of the Mechanics and Physics of Solids, 1960. **8**(2): p. 100-104.
44. Xie, D. and A.M. Waas, *Discrete cohesive zone model for mixed-mode fracture using finite element analysis.* Engineering Fracture Mechanics, 2006. **73**(13): p. 1783-1796.
45. Cui, W. and M.R. Wisnom, *A combined stress-based and fracture-mechanics-based model for predicting delamination in composites.* Composites, 1993. **24**(6): p. 467-474.
46. Feraren, P. and H.M. Jensen, *Cohesive zone modelling of interface fracture near flaws in adhesive joints.* Engineering Fracture Mechanics, 2004. **71**(15): p. 2125-2142.
47. Yang, Q.D., M.D. Thouless, and S.M. Ward, *Elastic–plastic mode-II fracture of adhesive joints.* International Journal of Solids and Structures, 2001. **38**(18): p. 3251-3262.
48. ABAQUS® Documentation. 2009, Dassault Systèmes: Vélizy-Villacoublay.
49. Zhu, Y., K.M. Liechti, and K. Ravi-Chandar, *Direct extraction of rate-dependent traction–separation laws for polyurea/steel interfaces.* International Journal of Solids and Structures, 2009. **46**(1): p. 31-51.
50. Campilho, R.D.S.G., M.F.S.F. de Moura, and J.J.M.S. Domingues, *Using a cohesive damage model to predict the tensile behaviour of CFRP single-strap repairs.* International Journal of Solids and Structures, 2008. **45**(5): p. 1497-1512.
51. Alfano, G. and M.A. Crisfield, *Finite element interface models for the delamination analysis of laminated composites: mechanical and computational issues.* International Journal for Numerical Methods in Engineering, 2001. **50**(7): p. 1701-1736.
52. Allix, O. and A. Corigliano, *Modeling and simulation of crack propagation in mixed-modes interlaminar fracture specimens.* International Journal of Fracture. **77**(2): p. 111-140.
53. Chen, J., *Predicting Progressive Delamination of Stiffened Fibre-Composite Panel and Repaired Sandwich Panel by Decohesion Models.* Journal of Thermoplastic Composite Materials, 2002. **15**(5): p. 429-442.
54. Chandra, N., H. Li, C. Shet, and H. Ghonem, *Some issues in the application of cohesive zone models for metal–ceramic interfaces.* International Journal of Solids and Structures, 2002. **39**(10): p. 2827-2855.
55. Kafkalidis, M.S. and M.D. Thouless, *The effects of geometry and material properties on the fracture of single lap-shear joints.* International Journal of Solids and Structures, 2002. **39**(17): p. 4367-4383.
56. Campilho, R.D.S.G., M.F.S.F. de Moura, and J.J.M.S. Domingues, *Numerical prediction on the tensile residual strength of repaired CFRP under different geometric changes.* International Journal of Adhesion and Adhesives, 2009. **29**(2): p. 195-205.
57. Pinto, A.M.G., A.G. Magalhães, R.D.S.G. Campilho, M.F.S.F. de Moura, and A.P.M. Baptista, *Single-Lap Joints of Similar and Dissimilar Adherends Bonded with an Acrylic Adhesive.* The Journal of Adhesion, 2009. **85**(6): p. 351-376.
58. Campilho, R.D.S.G., M.F.S.F.d. Moura, D.A. Ramantani, J.J.L. Morais, A.M.J.P. Barreto, and J.J.M.S. Domingues, *Adhesively Bonded Repair Proposal for Wood Members Damaged by Horizontal Shear Using Carbon-Epoxy Patches.* The Journal of Adhesion, 2010. **86**(5-6): p. 649-670.
59. Campilho, R.D.S.G., M.D. Banea, A.M.G. Pinto, L.F.M. da Silva, and A.M.P. de Jesus, *Strength prediction of single- and double-lap joints by standard and extended finite element modelling.* International Journal of Adhesion and Adhesives, 2011. **31**(5): p. 363-372.
60. Khoramishad, H., A.D. Crocombe, K.B. Katnam, and I.A. Ashcroft, *Predicting fatigue damage in adhesively bonded joints using a cohesive zone model.* International Journal of Fatigue, 2010. **32**(7): p. 1146-1158.
61. Daudeville, L. and P. Ladevèze, *A damage mechanics tool for laminate delamination.* Composite Structures, 1993. **25**(1–4): p. 547-555.

62. Voyiadjis, G.Z. and P.I. Kattan, *Damage mechanics*. 2005, New York: Marcell Dekker.
63. Raghavan, P. and S. Ghosh, *A continuum damage mechanics model for unidirectional composites undergoing interfacial debonding.* Mechanics of Materials, 2005. **37**(9): p. 955-979.
64. Wahab, M.M.A., I.A. Ashcroft, A.D. Crocombe, and S.J. Shaw, *Prediction of fatigue thresholds in adhesively bonded joints using damage mechanics and fracture mechanics.* Journal of Adhesion Science and Technology, 2001. **15**(7): p. 763-781.
65. Shenoy, V., I.A. Ashcroft, G.W. Critchlow, and A.D. Crocombe, *Fracture mechanics and damage mechanics based fatigue lifetime prediction of adhesively bonded joints subjected to variable amplitude fatigue.* Engineering Fracture Mechanics, 2010. **77**(7): p. 1073-1090.
66. Lemaitre, J., *Local approach of fracture.* Engineering Fracture Mechanics, 1986. **25**(5): p. 523-537.
67. Lemaitre, J. and J.L. Chaboche, *Mechanics of Solid Materials*. 1990: Cambridge University Press.
68. Sampaio, E.M., F. Luiz Bastian, and H.S. Costa Mattos, *A simple continuum damage model for adhesively bonded butt joints.* Mechanics Research Communications, 2004. **31**(4): p. 443-449.
69. Hua, Y., A.D. Crocombe, M.A. Wahab, and I.A. Ashcroft, *Continuum damage modelling of environmental degradation in joints bonded with EA9321 epoxy adhesive.* International Journal of Adhesion and Adhesives, 2008. **28**(6): p. 302-313.
70. Belytschko, T. and T. Black, *Elastic crack growth in finite elements with minimal remeshing.* International Journal for Numerical Methods in Engineering, 1999. **45**: p. 601-620.
71. Mohammadi, S., *Extended finite element method for fracture analysis of structures*. 2008, New Jersey, USA: Blackwell Publishing.
72. Moës, N., J. Dolbow, and T. Belytschko, *A finite element method for crack growth without remeshing.* International Journal for Numerical Methods in Engineering, 1999. **46**: p. 131-150.
73. Campilho, R.D.S.G., M.D. Banea, F.J.P. Chaves, and L.F.M.d. Silva, *eXtended Finite Element Method for fracture characterization of adhesive joints in pure mode I.* Computational Materials Science, 2011. **50**(4): p. 1543-1549.
74. Sukumar, N., N. Moës, B. Moran, and T. Belytschko, *Extended finite element method for three-dimensional crack modelling.* International Journal for Numerical Methods in Engineering, 2000. **48**: p. 1549-1570.
75. Daux, C., N. Moës, J. Dolbow, N. Sukumar, and T. Belytschko, *Arbitrary branched and intersecting cracks with the extended finite element method.* International Journal for Numerical Methods in Engineering, 2000. **48**: p. 1741-1760.
76. Moës, N. and T. Belytschko, *Extended finite element method for cohesive crack growth.* Engineering Fracture Mechanics, 2002. **69**(7): p. 813-833.
77. Elguedj, T., A. Gravouil, and A. Combescure, *Appropriate extended functions for X-FEM simulation of plastic fracture mechanics.* Computer Methods in Applied Mechanics and Engineering, 2006. **195**(7–8): p. 501-515.
78. Barbosa, N.G.C., R.D.S.G. Campilho, F.J.G. Silva, and R.D.F. Moreira, *Comparison of different adhesively-bonded joint types for mechanical structures.* Applied Adhesion Science, 2018. **6**(1): p. 15.
79. Moreira, P.M.G.P., A.M.P. de Jesus, A.S. Ribeiro, and P.M.S.T. de Castro, *Fatigue crack growth in friction stir welds of 6082-T6 and 6061-T6 aluminium alloys: A comparison.* Theoretical and Applied Fracture Mechanics, 2008. **50**(2): p. 81-91.
80. Campilho, R.D.S.G., D.C. Moura, D.J.S. Gonçalves, J.F.M.G. da Silva, M.D. Banea, and L.F.M. da Silva, *Fracture toughness determination of adhesive and co-cured joints in natural fibre composites.* Composites Part B: Engineering, 2013. **50**: p. 120-126.
81. de Sousa, C.C.R.G., *Comparação de técnicas analíticas e numéricas para previsão da resistência de juntas adesivas de sobreposição simples*. 2016, Tese de Mestrado em

Engenharia Mecânica - Ramo Construções Mecânicas. Instituto Superior de Engenharia do Porto: Porto.

82. Neto, J.A.B.P., R.D.S.G. Campilho, and L.F.M. da Silva, *Parametric study of adhesive joints with composites.* International Journal of Adhesion and Adhesives, 2012. **37**: p. 96-101.
83. Petrie, E.W., *Handbook of adhesives and sealants*. 2nd ed ed. 1999, New York: McGraw-Hill.
84. Campilho, R.D.S.G., M.D. Banea, J.A.B.P. Neto, and L.F.M. da Silva, *Modelling adhesive joints with cohesive zone models: effect of the cohesive law shape of the adhesive layer.* International Journal of Adhesion and Adhesives, 2013. **44**: p. 48-56.
85. Campilho, R.D.S.G., M.D. Banea, J.A.B.P. Neto, and L.F.M. da Silva, *Modelling of Single-Lap Joints Using Cohesive Zone Models: Effect of the Cohesive Parameters on the Output of the Simulations.* The Journal of Adhesion, 2012. **88**(4-6): p. 513-533.
86. Carvalho, U.T.F., *Modelação de juntas adesivas de sobreposição simples e dupla por modelos de dano coesivo com obtenção das leis coesivas pelo método direto*. 2016, Tese de Mestrado de Engenharia Mecânica - Ramo Contruções Mecânicas. Instituto Superior de Engenharia do Porto: Porto.
87. Faneco, T.M.S., *Caraterização das propriedades mecânicas de um adesivo estrutural de alta ductilidade*. 2014, Tese de Mestrado em Engenharia Mecânica - Ramo Materias e Tecnologias de Fabrico. Instituto Superior de Engenharia do Porto: Porto.
88. Campilho, R.D.S.G., M.F.S.F. de Moura, A.M.G. Pinto, J.J.L. Morais, and J.J.M.S. Domingues, *Modelling the tensile fracture behaviour of CFRP scarf repairs.* Composites Part B: Engineering, 2009. **40**(2): p. 149-157.
89. Alfano, G., *On the influence of the shape of the interface law on the application of cohesive-zone models.* Composites Science and Technology, 2006. **66**(6): p. 723-730.
90. Pocius, A.V., *Adhesion and Adhesives Technology, An Introduction*. 2nd Edition ed. 2002: Hanser.
91. Campilho, R.D.S.G., M.F.S.F. de Moura, and J.J.M.S. Domingues, *Modelling single and double-lap repairs on composite materials.* Composites Sci. Technol., 2005. **65**(null): p. 1948.
92. Andersson, T. and U. Stigh, *The stress–elongation relation for an adhesive layer loaded in peel using equilibrium of energetic forces.* International Journal of Solids and Structures, 2004. **41**(2): p. 413-434.
93. Leffler, K., K.S. Alfredsson, and U. Stigh, *Shear behaviour of adhesive layers.* International Journal of Solids and Structures, 2007. **44**(2): p. 530-545.
94. Högberg, J.L. and U. Stigh, *Specimen proposals for mixed mode testing of adhesive layer.* Engineering Fracture Mechanics, 2006. **73**(16): p. 2541-2556.
95. Campilho, R.D.S.G., A.M.G. Pinto, M.D. Banea, R.F. Silva, and L.F.M. da Silva, *Strength Improvement of Adhesively-Bonded Joints Using a Reverse-Bent Geometry.* Journal of Adhesion Science and Technology, 2011. **25**(18): p. 2351-2368.
96. de Moura, M.F.S.F., R.D.S.G. Campilho, and J.P.M. Gonçalves, *Pure mode II fracture characterization of composite bonded joints.* International Journal of Solids and Structures, 2009. **46**(6): p. 1589-1595.
97. de Moura, M.F.S.F., R.D.S.G. Campilho, and J.P.M. Gonçalves, *Crack equivalent concept applied to the fracture characterization of bonded joints under pure mode I loading.* Composites Science and Technology, 2008. **68**(10–11): p. 2224-2230.
98. Azevedo, J.C.S., *Determinação da tenacidade à fratura em tração (GIIC) de adesivos estruturais pelo ensaio End-Notched Flexure (ENF)*, in *Engenharia Mecânica*. 2014, Instituto Superior de Engenharia do Porto.
99. Faneco, T.M.S., *Caracterização das propriedades mecânicas de um adesivo estrutural de alta ductilidade*, in *Engenharia Mecânica*. 2014, Instituto Superior de Engenharia do Porto.

100. Nunes, S.L.S., R.D.S.G. Campilho, F.J.G. da Silva, C.C.R.G. de Sousa, T.A.B. Fernandes, M.D. Banea, and L.F.M. da Silva, *Comparative Failure Assessment of Single and Double Lap Joints with Varying Adhesive Systems.* The Journal of Adhesion, 2016. **92**(7-9): p. 610-634.
101. Alves, D.L., *Ligações adesivas com chanfro interior entre aderentes distintos*, in *Engenharia Mecânica*. 2016, ISEP: Porto.
102. Campilho, R.D.S.G., M.F.S.F. de Moura, and J.J.M.S. Domingues, *Stress and failure analyses of scarf repaired CFRP laminates using a cohesive damage model.* Journal of Adhesion Science and Technology, 2007. **21**(9): p. 855-870.
103. Moreira, R.D.F. and R.D.S.G. Campilho, *Strength improvement of adhesively-bonded scarf repairs in aluminium structures with external reinforcements.* Engineering Structures, 2015. **101**(Supplement C): p. 99-110.
104. Nunes, S.L.S., *Estudo comparativo da resistência à tração de juntas adesivas de sobreposição simples e dupla*. 2015.
105. Carvalho, U.T.F., *Modelação de juntas adesivas por modelos de dano coesivo utilizando o método direto*. 2016.